Theory of magnetic response in nodal semimetals

PhD Thesis

Theory of magnetic response in nodal semimetals

（ノーダル半金属における磁場応答の理論）

Intan Fatimah Hizbullah

Department of Physics

Graduate School of Science

Tohoku University

2018

Contents

Chapter 1

Introduction

1.1 Purpose of the study

In the ordinary metal, it is well-known that the magnetic susceptibility consists of Pauli paramagnetism (spin term) and Landau diamagnetism (orbital term). Pauli paramagnetism is positive magnetic susceptibility, while Landau diamagnetism is negative susceptibility. However, it is not always true when we have spin-orbit (SO) interaction in the system. The SO interaction may give rise to a new term of magnetic susceptibility, which is not the spin paramagnetism nor the orbital diamagnetism.

The purpose of study is to understand the magnetic response of various materials with strong spin-orbit coupling (SOC), including two-dimensional (2D) Rashba /Dresselhaus system, the 2D surface state of topological insulator, and three-dimensional (3D) nodal semimetals. We start with the well-known spin-orbit coupled system, i.e. 2D electron gas (2DEG) with Rashba and Dresselhaus SOC. In both cases, the spin-orbit interaction is induced by the inversion symmetry breaking. The Rashba effect occurs when there is structural inversion asymmetry in the junction of semiconductor hetero-structures [1, 2], while the Dresselhaus effect occurs when the asymmetry exist in bulk crystal structure.[3] Although the energy dispersion at zero magnetic field is essentially equivalent in both Rashba and Dresselhaus systems, but the spin texture on the momentum space is completely different between them. We will show that this leads to a significant difference in the spin-orbit cross term in the magnetic

susceptibility.

Moreover, there are a variety of novel topological materials in which the spin orbit coupling is essential, such as topological insulator, the Dirac semimetal, and the Weyl semimetal. They are new, but the magnetic response is not well known. The topological insulator is a bulk insulator with topological surface states.[4, 5, 6, 7, 8] The Weyl and Dirac semimetals are the systems with 3D gapless spectrum where the energy bands touch at isolated points in the momentum space.[9, 61, 62, 63, 64, 10, 14, 16, 18, 19, 23]. We expand our standard knowledge of paramagnetism/diamagnetism to those novel materials by calculating the magnetic susceptibility.

This thesis will be organized as follows: In Chapter 2, we calculate the magnetic susceptibility for 2DEG with Rashba SOC and Dresselhaus SOC, and also the 2D Dirac surface states of the topological insulator. In Chapter 3, we present the detailed calculation of the magnetic response for 3D Dirac/Weyl semimetals. Lastly, the conclusion will be presented in Chapter 4.

1.2 Background

1.2.1 Magnetism of metals

In the ordinary metal, it is well-known that the magnetic susceptibility consists of Pauli paramagnetism and Landau diamagnetism. Pauli paramagnetism is caused by the spin magnetic moment, while the Landau diamagnetism originates from the orbital cyclotron motion. In the Pauli paramagnetism, an external magnetic field shifts the energy levels up and down by $\pm\mu_B H$, where μ_B is Bohr magneton, H is the magnetic field applied. This immediately results in different numbers in the up spins and down spins at the equilibrium and thus the system has a finite magnetization as a whole. In Landau diamagnetism, on the other hand, the electrons makes a circular motion under the Lorentz force, and it gives the magnetization. In the quantum mechanics, the energy spectrum is quantized into the discrete levels $(n+1/2)\hbar\omega_c$ where n is integer and the spacing width is $\hbar\omega_c$ between the levels. $\hbar$ is Planck constant h divided by 2π and ω_c is the cyclotron frequency. This is called the Landau quantization and this correctly explains the diamagnetic behavior. [24] For free electron, the magnitude of Landau diamagnetism is 3 times smaller than the Pauli paramagnetism. In total,

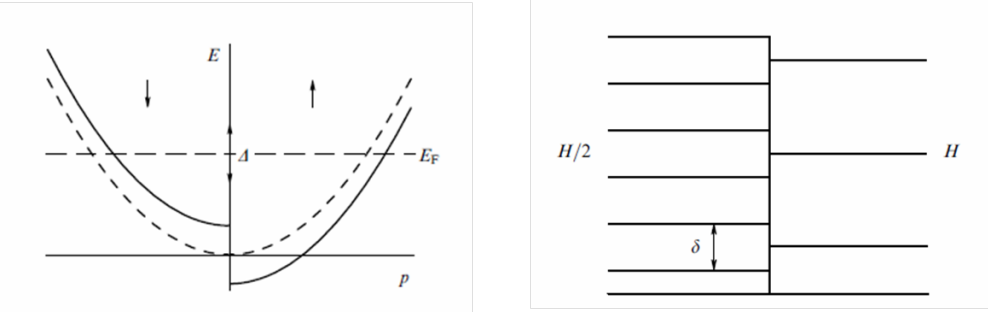

Figure 1.1: Energy band shifting in Pauli paramagnetism (left) and energy quantization in Landau diamagnetism (right). [26]

therefore, the magnetic susceptibility is paramagnetic.

The above classic argument applies to the spin-independent free electron system with the quadratic dispersion $E = p^2/2m$. If the system has the spin-orbit interaction, then the spin magnetism and the orbital magnetism cannot be treated independently and we need a different approach to describe the magnetic response. In this thesis, we show that the magnetic susceptibility in SOC is generally composed of three terms; the spin-spin term ($\chi_{\rm spin}$), the orbital-orbital term ($\chi_{\rm orb}$), and also the spin-orbital term ($\chi_{\rm SO}$). We calculate those three terms for different electronic systems introduced in the following, and argue the characteristic property of each term in a systematic manner.

1.2.2 Rashba / Dresselhaus system

As mentioned before, the Pauli paramagnetism comes from the contribution of spins and Landau diamagnetism comes from the orbital contribution. However it's not always true if we have system having spin-orbit coupling (SOC). The SOC effect may give rise the cross term of spin-orbit contribution. Here we explain the well-known spin-orbit coupled system, i.e. 2DEG with Rashba and Dresselhaus SOC. In both cases, the spin-orbit interaction is induced by the inversion symmetry breaking.

The Rashba effect occurs when there is structural inversion asymmetry in the junction of semiconductor hetero-structures. This effect was proposed by Bychkov-Rashba to explain the splitting phenomena at $GaAs - Al_xGa_{1-x}As$ heterostuctures in

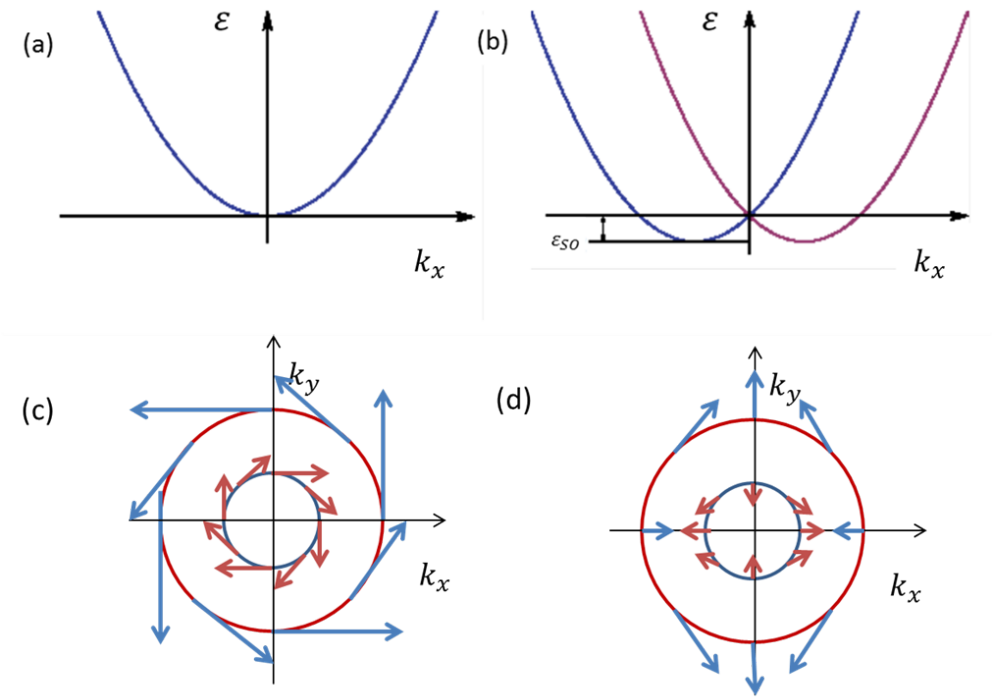

Figure 1.2: Side view:(a). Band dispersion of 2DEG without SOC, (b). band dispersion for 2DEG with SOC. Top view: (c). Spin orientation for 2DEG with Rashba SOC, (d). spin orientation for 2DEG with Dresselhaus SOC.

n- and p-type layers.[1, 2] Recently, experimental observations of giant Rashba spin-orbit coupling have been reported.[30, 31, 32, 33, 34] Theoretical research of magnetic response in 2DEG with the contribution of Rashba effect had been recently calculated. [35, 36]The Dresselhaus effect occurs when the asymmetry exist in crystal structure of the bulk material. This theory was proposed by Dresselhaus in 1955 to describe the SOC effect in zinc blende structures material.[3]

In the Rashba / Dresselhaus spin orbit interaction, the electrons feel the effective Zeeman field depending on the electronic momentum, so that the spin direction correlates with the momentum direction. Although the spectrum at zero magnetic field is essentially equivalent in both Rashba and Dresselhaus systems, the spin texture in the momentum space is completely different as illustrated in Fig. 1.2. Specifically, if

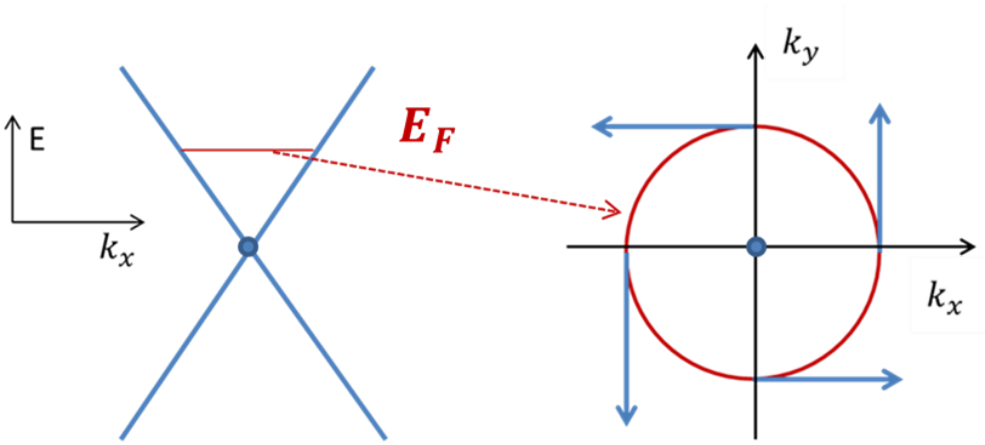

Figure 1.3: The cone shaped band dispersion of the surface of topological insulator (left). The view of the Fermi surface from the top (right). The spin's vector is perpendicular to momentum k.

we rotate the equi-energy contour in the momentum space in the clock-wise direction, then the spin also rotates in the clockwise direction in Rashba system, while in the counter-clockwise direction in the Dresselhaus system. In that sense, the two systems have opposite "chirality" (or "handedness") of the spin texture. The similar chiral spin texture is also found in the surface states of the topological insulator. [7, 8] The topological insulators are electronic systems which have a bulk band gap but also have protected conducting states on the surface. The 3D topological insulators such as Bi_2Se_3 and Bi_2Te_3, the surface state band is approximates the 2D Dirac cone, where the spin direction correlates with the momentum as in Fig. 1.3.

In this thesis, we calculate the magnetic susceptibility of Rashba /Dresselhaus systems and also 2D Dirac mode for the surface states of the 2D topological insulator. We demonstrate that the spin-momentum relationship makes an essential difference in the spin-orbit cross term, and determines the amplitude and sign of the total susceptibility.

1.2.3 Weyl / Dirac semimetals

In this thesis, we also theoretically investigate the magnetic response of three-dimensional (3D) gapless electron systems. The 3D version of the gapless band structure was the-

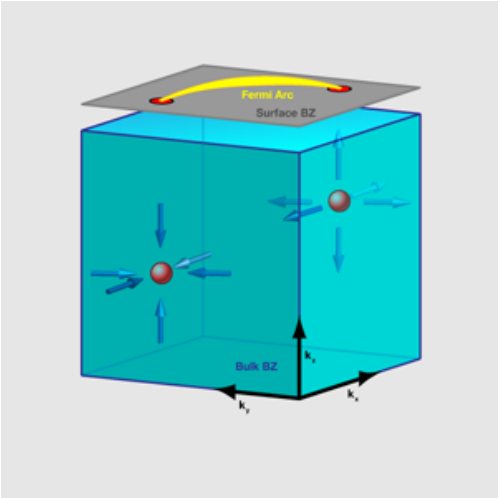

Figure 1.4: Three dimensional schematic image of the Weyl semimetal in momentum space. [47]

oretically proposed by [9, 61, 62, 63, 64, 10, 14, 16, 18, 19, 23]. In very recent experiments, such 3D gapless electron systems were actually realized in various materials [46, 58, 52, 53, 54, 55].

In 2D gapless electron system (e.g., graphene), the low energy effective theory at point degeneracies between the conduction and valence bands takes the form, $H(\mathbf{k}) = v(k_x\sigma_x + k_y\sigma_y)$ where σ_x, σ_y are the Pauli matrices and v is the velocity parameter. In 3D, the analogous Hamiltonian is $H(\mathbf{k}) = v(k_x\sigma_x + k_y\sigma_y + k_z\sigma_z)$ with all three Pauli matrices, and it is called a Weyl Hamiltonian as it describes a pair of linear bands degenerating at a point. When the two different Weyl points happen to merge at a single momentum, the system is called the Dirac semimetal, since the effective Hamiltonian is given by 4×4 Dirac Hamiltonian around the four-fold degenerate point. If the Weyl points are isolated in the momentum space, on the contrary, the system is called the Weyl-semimental, and the effective Hamiltonian at each Weyl point is given by 2×2 Weyl Hamiltonian. The schematic image of Weyl semimetal is shown in Fig.1.4 [47].

Therefore, we have three different categories of 3D band structures, the trivial insulator (fully gapped), the Dirac semimetal and the Weyl semimetal. The Dirac

semimetal exists on the phase boundary between the trivial insulator and the Weyl semimetal. The Dirac semimetal can generally occur when the system has both the time-reversal (T) symmetry and the spacial-inversion (I) symmetry and the Weyl semimetal can be obtained by breaking either of T or I symmetries [9]. In recent exeperiments these three-dimensional gapless band structures are actually realized in specific compounds. The Dirac semimetal phase was found in β-cristiobalite BiO_2, Cd_3As_2 and Na_3Bi [46, 58, 52], and the experimental realization of a Weyl semimetal state have been recently reported in TaAs and NbAs. [53, 54, 55, 56]

The existence of Dirac points near the Fermi level is responsible for various unusual physical properties. One of the most spectacular examples is the magnetic susceptibility, which is quite distinct from the conventional Landau diamagnetism. In two-dimenisional graphene, the electronic orbital diamagnetism contains a singularity expressed as a delta function in Fermi energy, which diverges at Dirac point where the two bands stick, and vanishes otherwise. [41, 42, 43] The similar calculation of the orbital magnetism was also done for 3D Dirac Hamiltonian, [50] and it was shown that the susceptibility in the gapless case becomes a logarithmic function in the Fermi energy.

The result seems to directly apply to the Dirac and Weyl semimetals, but there is an important difference between the real relativistic Dirac Hamiltonian and the effective Dirac Hamiltonian in the solid state physics. In the Dirac and Weyl semimetals, the external magnetic field B enters the Hamiltonian in two independent manners, one in the orbital part where $\mathbf{p}$ is changed to $\mathbf{p}+e\mathbf{A}$ with the vector potential $\mathbf{A}$, and the other in the spin Zeeman term $g\mu_B B$, where g is the g-factor and μ_B is the Bohr magneton. The two-different magnetic field terms give rise to the different terms in the magnetic susceptibility, the spin-spin term, the orbital-orbital term, and the spin-orbital cross term, which are not captured in the previous calculation including only the orbital part. In this thesis, we calculate those components and correctly describe the total magnetic response in the three-dimensional gapless semimetals. First we calculate analytically the Landau level spectrum of 4×4 linear Hamiltonian which covers Dirac and Weyl semimetal phases. Then we take the derivative of the thermodynamic potential to get the magnetic susceptibility.

Chapter 2

2DEG with Rashba/Dresselhaus SOC and 2D Dirac System

In this chapter, we calculate the magnetic susceptibility of Rashba /Dresselhaus systems and also 2D Dirac mode for the surface states of the 2D topological insulator. We show that the spin-momentum relationship governs the sign the spin-orbit cross term, and that significantly affects the amplitude and sign of the total susceptibility.

2.1 Hamiltonian and Landau Levels

2.1.1 2DEG with Rashba and Dresselhaus Spin-Orbit Coupling

We start from the Hamiltonian of 2DEG with mass m without magnetic field written as

$$\mathcal{H}_0 = \frac{\mathbf{p}^2}{2m}, \tag{2.1}$$

From the equation we know the energy band is a parabolic curve in momentum (Fig. (2.1) (a)). Next, we consider the Hamiltonian of 2DEG with Rashba SOC in presence of magnetic field B parallel to z axis,[2]

$$\mathcal{H}_R = \frac{\pi^2}{2m} - \frac{\lambda_R}{\hbar}(\pi_x\sigma_y - \pi_y\sigma_x) + b\sigma_z, \tag{2.2}$$

The Zeeman term is added as the consequence of the magnetic field presence in the system. In the Dresselhaus SOC case, we only consider the linear Dresselhaus SO

term. The Hamiltonian is written as [49]

$$\mathcal{H}_D = \frac{\pi^2}{2m} + \frac{\lambda_D}{\hbar}(\pi_x\sigma_x - \pi_y\sigma_y) + b\sigma_z. \tag{2.3}$$

Here $\sigma_x, \sigma_y, \sigma_z$ is Pauli matrices, $\lambda_R(\lambda_D)$ is Rashba (Dresselhaus) coefficient, and

$$\pi = \mathbf{p} + e\mathbf{A}, \tag{2.4}$$

where $\mathbf{A}$ is vector potential giving in the magnetic field by $\mathbf{B} = \nabla \times \mathbf{A}$. Here note that b is also dependent on the external magnetic field B as

$$b = \frac{1}{2}g\mu_B B, \tag{2.5}$$

where and g is g-factor and $\mu_B = e\hbar/(2m_0)$ is the Bohr magneton, and m_0 is the bare electron mass.

When we add Rashba (Dresselhaus) term into the Hamiltonian, the energy band splits into two bands crossing at zero point forming a single Dirac point like state as in graphene and other Dirac materials (see Fig. 2.1 (b)). Where ε_{SO} here is spin-orbit energy proportional to Rashba(Dresselhaus) coefficient $\lambda_R(\lambda_D)$.

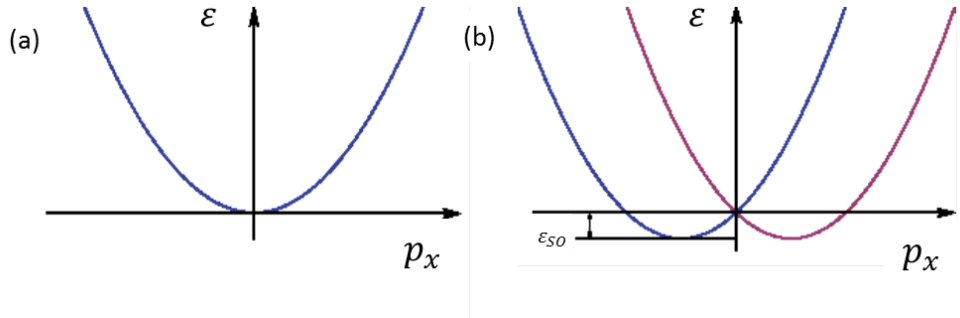

Figure 2.1: Energy band of 2DEG (a) without Rashba (Dresselhaus) SOC, and (b) with Rashba(Dresselhaus) SOC.

To calculate the Landau level we define a lower and uppering operators as

$$a^\dagger = \frac{1}{\sqrt{2e\hbar B}}(\pi_x + i\pi_y) \tag{2.6}$$

$$a = \frac{1}{\sqrt{2e\hbar B}}(\pi_x - i\pi_y), \tag{2.7}$$

and we rewrite the Hamiltonian as

$$\mathcal{H}_{R(n\leq 1)} = \begin{bmatrix} \hbar\omega_c(a^\dagger a + \frac{1}{2}) + b & \frac{\sqrt{2}\lambda_R}{l_B} ia \\ -\frac{\sqrt{2}\lambda_R}{l_B} ia^\dagger & \hbar\omega_c(a^\dagger a + \frac{1}{2}) - b \end{bmatrix}. \tag{2.8}$$

These operators operate on the Landau-level wave function ϕ_n as $a\phi_n = \sqrt{n}\phi_{n-1}$ and $a^\dagger\phi_n = \sqrt{n+1}\phi_{n+1}$. In Rashba system the eigenfunction can be written as $(c_1\phi_{n-1},\, c_2\phi_n)$ for $n \geq 1$, the Hamiltonian matrix for the vector (c_1, c_2) then becomes

$$\mathcal{H}_{R(n\leq 1)} = \begin{bmatrix} \hbar\omega_c(n - \frac{1}{2}) + b & i\frac{\sqrt{2}\lambda_R}{l_B}\sqrt{n} \\ -i\frac{\sqrt{2}\lambda_R}{l_B}\sqrt{n} & \hbar\omega_c(n + \frac{1}{2}) - b \end{bmatrix}, \tag{2.9}$$

This gives the two energy levels

$$\varepsilon_{R_{sn}} = n\hbar\omega_c + s\sqrt{(\frac{1}{2}\hbar\omega_c - b)^2 + (\frac{\sqrt{2n}\lambda_R}{l_B})^2} \tag{2.10}$$

where $s = \pm$, $\omega_c = \frac{eB}{m^*}$ is the cyclotron frequency and $l_B = \sqrt{\frac{\hbar}{eB}}$ is the magnetic length. For $n = 0$, the wave function is written as $(0,\, c_2\phi_0)$ which gives the only one levels

$$\varepsilon_{R_{n=0}} = \frac{1}{2}\hbar\omega_c - b. \tag{2.11}$$

The level ε_s can be viewed as the $n = 0$ part of $\varepsilon_{R,sn}$ in Eq. (2.10), but $s = -$ part is missing.

In Dresselhaus system the eigenfunction can be written as $(c_3\phi_n,\, c_4\phi_{n-1})$ for $n \geq 1$, the Hamiltonian matrix for the vector (c_3, c_4) then becomes

$$\mathcal{H}_{D(n\leq 1)} = \begin{bmatrix} \hbar\omega_c(n + \frac{1}{2}) + b & \frac{\sqrt{2}\lambda_D}{l_B}\sqrt{n} \\ \frac{\sqrt{2}\lambda_D}{l_B}\sqrt{n} & \hbar\omega_c(n - \frac{1}{2}) - b \end{bmatrix}, \tag{2.12}$$

This gives the two energy levels

$$\varepsilon_{D_{sn}} = n\hbar\omega_c + s\sqrt{(\frac{1}{2}\hbar\omega_c + b)^2 + (\frac{\sqrt{2n}\lambda_D}{l_B})^2} \tag{2.13}$$

where $s = \pm$. For $n = 0$, the wave function is written as $(c_3\phi_0, 0)$ which gives the only one levels

$$\varepsilon_{D_{n=0}} = \frac{1}{2}\hbar\omega_c + b. \tag{2.14}$$

The level ε_s can be viewed as the $n = 0$ part of $\varepsilon_{D,sn}$ in Eq. (2.13), but $s = -$ part is missing. Note that Eqs. (2.9) and (2.12) differ only in the sign in front of of b.

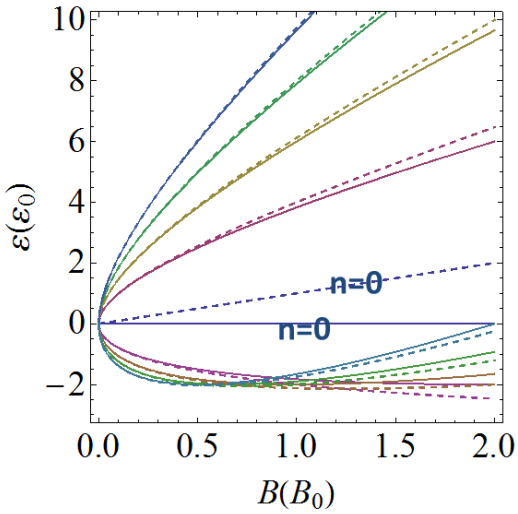

Figure 2.2: Landau level spectrum of Rashba system (solid lines) and Dresselhaus (dashed lines) system for $\lambda_R = \lambda_D = 2\sqrt{\frac{\hbar^3 eB_0}{m^{*2}}}$ and $g_m = m_0/m^*$. Where B_0 is unit of magnetic field.

Fig. 2.2 is the plot of Landau level for Rashba system (solid lines) and Dresselhaus system (dashed lines) with $\lambda_R = \lambda_D$ and the same g-factor. Their energy levels in $B \to 0$ limit are differ only in $n = 0$, while all other levels are almost degenerate.

2.1.2 2D Dirac System

Now we consider the 2D Dirac Hamiltonian which describes the surface state of the 3D topological insulator. It is similar to the Rashba /Dresselhaus system, while the p^2 term is absent.

The Hamiltonian is,

$$\mathcal{H}^R_{Dirac} = \begin{bmatrix} 0 & vi(p_x - ip_y) \\ -vi(p_x + ip_y) & 0 \end{bmatrix} \tag{2.15}$$

and

$$\mathcal{H}^D_{Dirac} = \begin{bmatrix} 0 & v(p_x + ip_y) \\ v(p_x - ip_y) & 0 \end{bmatrix} \tag{2.16}$$

which are analogous to the Rashba and Dresselhaus systems, respectively. It looks similar to graphene, but here the vector components correspond to the real spin degree of freedom. The two Hamiltonians have different spin-texture as a function of momentum. The surface band of the typical topological insulators such as Bi_2Se_3 corresponds to the case Eq.(2.15). The differences between those Hamiltonians are the imaginary parts in the off diagonal parts and the sign in front of p_y. Although the Hamiltonians are different, their energy bands are identical, written as

$$\varepsilon_s^{R,D} = svp \tag{2.17}$$

where $s = \pm$.

We can see the plot for the energy bands in Fig. 2.3. We have Dirac point at (0,0).

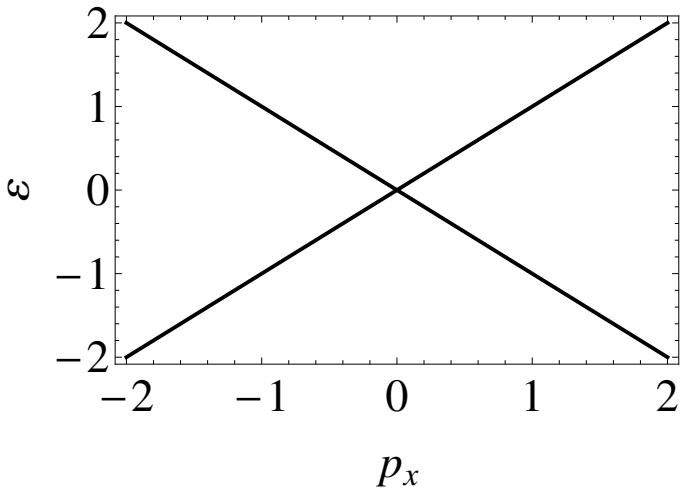

Figure 2.3: Energy bands for 2D Dirac systems [Eqs. (2.15) and (2.16)] at zero magnetic field.

The Hamiltonian in presence of external magnetic field B in z axis is

$$\mathcal{H}^R_{Dirac} = \begin{bmatrix} b & vi(\pi_x - i\pi_y) \\ -vi(\pi_x + i\pi_y) & -b \end{bmatrix} \tag{2.18}$$

and

$$\mathcal{H}^D_{Dirac} = \begin{bmatrix} b & v(\pi_x + i\pi_y) \\ v(\pi_x - i\pi_y) & -b \end{bmatrix} \tag{2.19}$$

for Rashba dan Dresselhaus case respectively.

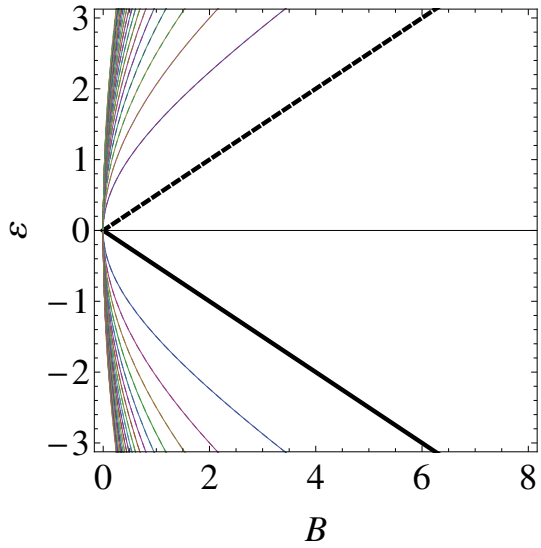

Figure 2.4: Landau levels for 2D Dirac systems. Solid and dashed thick lines are the $n = 0$ level for the Rashba type [Eq. (2.15)], and Dresselhaus type [Eq. (2.16)], respectively. Thin curves are $n \neq 0$ levels which are shared by the two cases.

The Landau levels for both cases are identical for $n \neq 0$

$$\varepsilon_s^{R,D} = s\sqrt{(b)^2 + v^2 2\hbar e B n}. \tag{2.20}$$

For $n = 0$ the Landau level is,

$$\varepsilon_{n=0}^{R,D} = \alpha_{R,D} b \tag{2.21}$$

where,

$$\alpha_{R,D} = \begin{cases} \alpha_R = -1 & \text{for Rashba type,} \\ \alpha_D = 1 & \text{for Dresselhaus type.} \end{cases}$$

2.2 Magnetic susceptibility

The magnetic susceptibility can be derived from the thermodynamic potential. The thermodynamic potential of the system at temperature T is written as

$$\Omega = -\frac{1}{\beta}\sum_{\alpha} \ln[1 + \exp -\beta(\varepsilon_\alpha - \zeta)], \tag{2.22}$$

where α is the index labeling the all eigenstates of the system, $\beta = 1/k_B T$, and ζ is the chemical potential. The magnetization is then given by

$$M = -\frac{\partial \Omega}{\partial B} = -\left(\frac{\partial \Omega}{\partial B_{\text{spin}}} + \frac{\partial \Omega}{\partial B_{\text{orb}}}\right). \tag{2.23}$$

The magnetic susceptibility is given by three components

$$\begin{aligned} \chi &= -\left.\frac{\partial M}{\partial B}\right|_{B=0} \\ &= \left[-\frac{\partial^2 \Omega}{\partial B_s^2} - 2\frac{\partial^2 \Omega}{\partial B_s \partial B_{orb}} - \frac{\partial^2 \Omega}{\partial B_{orb}^2}\right]_{B=0} \\ &\equiv \chi_{spin} + \chi_{so} + \chi_{orb}. \end{aligned} \tag{2.24}$$

We analytically derived the magnetic susceptibility using the Landau level spectrum Eq. (2.10) and Eq. (2.11). The thermodynamic potential in Eq. (2.22) per unit volume can be written as,

$$\begin{aligned} \Omega &= -\frac{1}{\beta}\frac{1}{2\pi l_B^2}\sum_{s=\pm}\sum_{n=0}^{\infty}\varphi[\varepsilon_{\mu s n}] \\ &\quad \left(1 - \delta_{n0}\frac{1-\tau_s}{2}\right), \end{aligned} \tag{2.25}$$

where

$$\varphi(\varepsilon_{\mu s n}) = \ln[1 + \exp -\beta(\varepsilon_{\mu s n} - \zeta)], \tag{2.26}$$

$l_B = \sqrt{\hbar/(eB_{\text{orb}})}$ is the magnetic length, ζ is the chemical potential.

2.2.1 2DEG with Rashba and Dresselhaus Spin-Orbit Coupling

The energy defined as,

$$\varepsilon_{\mu s n} = x_n + s\sqrt{(\Delta x/2 + \mu b)^2 + x_n x_{SO}} \tag{2.27}$$

with

$$x_n = n\Delta x, \quad \Delta x = 2\hbar e B_{\text{orb}}, \quad x_{SO} = \frac{2m^*\lambda_{SO}^2}{\hbar}. \tag{2.28}$$

Here λ_{SO} is Rashba(or Dresselhaus) constant, $\lambda_{R(or D)}$. The variable $\mu = \pm 1$ denotes Rashba and Dresselhaus systems as we already know that the difference of their energy

level is the sign in front of b,

$$\mu = \begin{cases} -1 & \text{for Rashba system,} \\ 1 & \text{for Dresselhaus system.} \end{cases} \tag{2.29}$$

We also introduced the variable $\tau_s = \pm 1$ as

$$\tau_s = \begin{cases} -1 & \text{when } \varepsilon_{s0} = -\varepsilon_0, \\ 1 & \text{when } \varepsilon_{s0} = \varepsilon_0. \end{cases} \tag{2.30}$$

Equivalently, we have $\tau_s = +1$ when the Landau level sequence of (s) start from $n = 0$, while $\tau_s = -1$ when it start from $n = 1$ (i.e., the $n = 0$ level is missing).

In small magnetic field, using the Euler-Maclaurin formula, the thermodynamic potential can be expanded in power of $B_{\rm orb}$ as

$$\Omega = \Omega_0 + \alpha_1(B_{\rm orb}) + \alpha_2(B_{\rm orb}^2) + \mathcal{O}(B_{\rm orb}^3) \tag{2.31}$$

where

$$\Omega_0 = -\frac{1}{\beta}\frac{1}{2\pi l_B^2}\sum_{s=\pm}\int_0^\infty \varphi(x,0)dx, \tag{2.32}$$

$$\begin{aligned} \alpha_1 &= -\frac{1}{\beta}\frac{1}{2\pi l_B^2}\sum_{s=\pm}\frac{e\hbar}{m^*}\left(\frac{\tau_s}{2}\varphi(0,0)\right. \\ &\quad \left. + \int_0^\infty \frac{\partial\varphi(x,\Delta x)}{\partial \Delta x}\bigg|_{\Delta x=0} dx\right) \end{aligned} \tag{2.33}$$

Eq. (2.33) expresses the contribution of spin-orbit part. The first term in the bracket tells us that SO term is solely dependent of n=0 Landau level.

$$\begin{aligned} \alpha_2 &= -\frac{1}{\beta}\frac{1}{2\pi l_B^2}\sum_{s=\pm}\frac{1}{2}\left(\frac{e\hbar}{m^*}\right)^2 \\ &\quad \left(\int_0^\infty \frac{\partial^2\varphi(x,\Delta x)}{\partial \Delta x^2}\bigg|_{\Delta x=0} dx\right. \\ &\quad + \frac{\tau_s \partial\varphi(0,\Delta x)}{\partial \Delta x}\bigg|_{\Delta x=0} \\ &\quad \left. -\frac{1}{12}\frac{\partial\varphi(x,0)}{\partial x}+\bigg|_{x=0}\right), \end{aligned} \tag{2.34}$$

Then we have,

$$\begin{aligned} \chi_{\rm orb} &= -2\alpha_2, \quad \chi_{\rm spin} = -\frac{\partial^2\Omega_0}{\partial B_{\rm spin}} \\ \chi_{\rm SO} &= -2\left.\frac{\partial\alpha_1}{\partial B_{\rm spin}}\right|_{B_{\rm spin}=0} \end{aligned} \tag{2.35}$$

Here we expect that only $\chi_{\rm SO}$ has opposite signs in Rashba and Dresselhaus systems, because it is the first derivative in b. While $\chi_{\rm spin}$ and $\chi_{\rm orb}$ is even-number (2 or 0) derivative in b, so the sign of b doesn't change the results.

Finally, we get the magnetic susceptibility as

$$\begin{aligned}\chi^*_{\rm orb} &= \frac{1}{2}\sqrt{1+\frac{\varepsilon_F}{\varepsilon_{\rm SO}}}\theta(-\varepsilon_F)\theta(\varepsilon_F+\varepsilon_{SO}) \\ &\quad -\frac{1}{6}\theta(\varepsilon_F)-\frac{2}{3}\varepsilon_{\rm SO}\delta(\varepsilon_F),\end{aligned} \tag{2.36}$$

and

$$\begin{aligned}\chi^*_{\rm spin} &= \frac{1}{2}g_m^2\sqrt{1+\frac{\varepsilon_F}{\varepsilon_{\rm SO}}}\theta(-\varepsilon_F)\theta(\varepsilon_F+\varepsilon_{\rm SO}) \\ &\quad +\frac{1}{2}\theta(\varepsilon_F)g_m^2,\end{aligned} \tag{2.37}$$

where

$$g_m=\frac{gm^*}{2m_0}, \tag{2.38}$$

$\chi^*=\chi/\chi_0$, and

$$\chi_0=\frac{e^2}{2\pi m^*} \tag{2.39}$$

is unit of susceptibility and

$$\varepsilon_{\rm SO}=\frac{m^*\lambda_R^2}{2\hbar^2}. \tag{2.40}$$

$\chi_{\rm spin}$ and χ_{orb} are completely identical for both systems if if they share the equal ε_{SO}. Our stressing point is that χ_{SO} comes with opposite signs, written as

$$\chi^*_{\rm SO} = \mu g_m\sqrt{1+\frac{\varepsilon_F}{\varepsilon_{SO}}}\theta(-\varepsilon_F)\theta(\varepsilon_F+\varepsilon_{SO}). \tag{2.41}$$

The sign of μ will change as the system changes.

The difference of χ_{SO} in both systems results the difference of total magnetic susceptibility, expressed as

$$\begin{aligned}\chi^*_{\rm Total} &= \frac{1}{2}\sqrt{1+\frac{\varepsilon_F}{\varepsilon_{SO}}}(g_m+\mu)^2\theta(-\varepsilon_F)\theta(\varepsilon_F+\varepsilon_{SO}) \\ &\quad +\frac{1}{2}(g_m^2-\frac{1}{3})^2\theta(\varepsilon_F)-\frac{2}{3}\varepsilon_{SO}\delta(\varepsilon_F)\end{aligned} \tag{2.42}$$

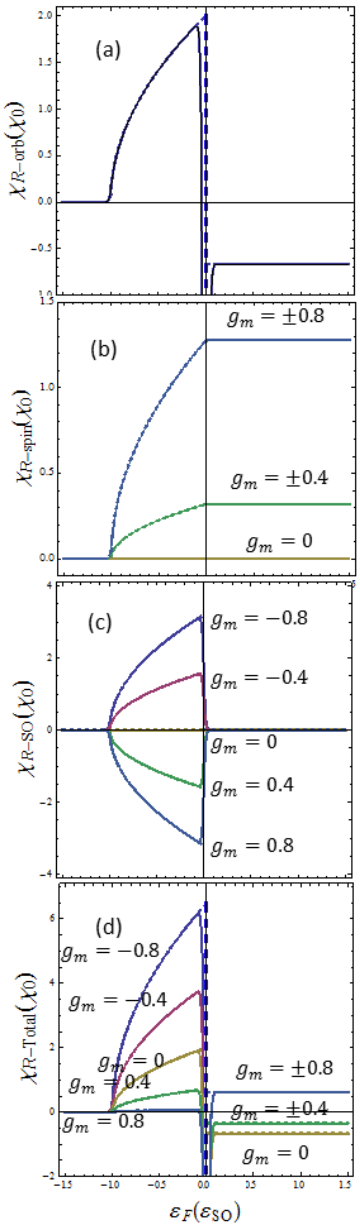

Figure 2.5: Magnetic Susceptibility for Rashba system (χ_R):(a) $\chi_{R_{\mathrm{orb}}}$ (b) $\chi_{R_{\mathrm{spin}}}$ (c) $\chi_{R_{\mathrm{SO}}}$ (d)$\chi_{R_{\mathrm{Total}}}$. Dashed lines are analytical results and solid lines are numerical results with $k_BT = 0.01\varepsilon_{\mathrm{SO}}$.

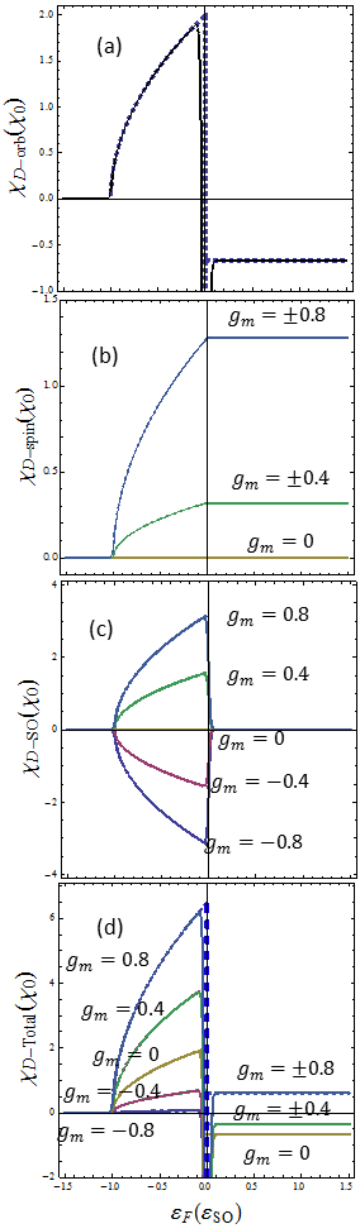

Figure 2.6: Magnetic Susceptibility for Dresselhaus system (χ_D):(a) $\chi_{D_{\mathrm{orb}}}$ (b) $\chi_{D_{\mathrm{spin}}}$ (c) $\chi_{D_{\mathrm{SO}}}$ (d)$\chi_{D_{\mathrm{Total}}}$. Dashed lines are analytical results and solid lines are numerical results with $k_B T = 0.01\varepsilon_{\mathrm{SO}}$.

2.2.2 2D Dirac

Now, we focus on The Dirac cone in Rashba and Dresselhaus case.

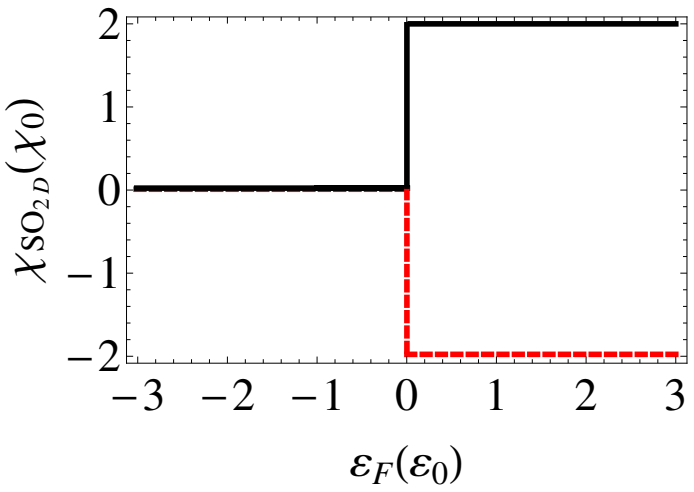

Figure 2.7: $\chi_{\rm SO}$ for Rashba(solid black line) and Dresselhaus(dashed red lines) 2D Dirac cone.

The energy defined as,

$$\varepsilon_{sn}^{R,D} = s\sqrt{b^2 + x_n} \tag{2.43}$$

with

$$x_n = n\Delta x, \quad \Delta x = 2v^2\hbar e B_{\rm orb}. \tag{2.44}$$

The magnetic susceptibility are,

$$\chi_{\rm SO}^{R,D} = -\alpha_{R,D}\frac{g\mu_B e}{\pi\hbar} \\ (-\theta(-|\varepsilon_F|) + 2\theta(\varepsilon_F)) \tag{2.45}$$

2.3 Discussion

In Fig. 2.5 and Fig. 2.6, we show the magnetic susceptibility as a function of the Fermi energy ε_F in 2D Rashba and Dresselhaus systems, respectively. Here (a) the orbital component, (b) the spin component, (c) the spin-orbit component, and (d)

the total susceptibility are plotted in separate panels. We can see that Rashba and Dresselhaus systems have identical orbital and spin susceptibility for $\lambda_R = \lambda_D$. The orbital susceptibility $\chi_{\rm orb}$ is positive (paramagnetic) in $\varepsilon_F < 0$, and it diverges to the negative infinity at $\varepsilon_F = 0$, and becomes constant in $\varepsilon_F > 0$. The divergence at zero energy is related to the band crossing point in the energy bands of zero magnetic field. This crossing point resembles Dirac point in graphene case. It has been shown that the orbital magnetic susceptibility of graphene diverges at zero energy [38]. The spin magnetic susceptbility $\chi_{\rm spin}$ is always paramagnetic due to its dependency of g^2. In negative Fermi energy it is an increasing function of Fermi energy, and it becomes constant in positive Fermi energy.

The difference of Rashba case and Dresselhaus case comes from the spin-orbit cross susceptibility, $\chi_{\rm SO}$. The sign of the spin-orbit magnetic susceptibility is completely opposite in Rashba and Dresselhaus systems, as argued in Eq. (2.41) and also seen in panel (c) of Figs. 2.5 and 2.6. $\chi_{\rm SO}$ is linear in g_m, so it is diamagnetic or paramagnetic depending on g_m. The $\chi_{\rm SO}$ is solely determined by $n = 0$ Landau level, while other susceptibility components depend on the whole Landau level spectrum. Indeed, the sign of the energy of $n = 0$ Landau level is opposite in Rashba and Dresselhaus systems, while all other Landau levels are just identical. This fact agrees with that the difference between Rashba and Dresselhaus systems is only found in $\chi_{\rm SO}$.

The difference in $\chi_{\rm SO}$ significantly affects the total magnetic susceptiblity. We show the total susceptibilities for the Rashba and Dresselhaus systems in (d) of Figs. 2.5 and 2.6. In $\varepsilon_F < 0$, the total magnetic susceptibility is always paramagnetic as is obvious from the first term of Eq. (2.42). In $\varepsilon_F > 0$, the total susceptibility is purely given by the $\chi_{\rm orb}$ and $\chi_{\rm spin}$ just as in the conventional metal without SOC, and it can be paramagnetic or diamagnetic depending on g-factor. The central delta-function peak is orbital effect, and it always exists independently of g_m.

In 2D Dirac case, the Rashba type and Dresselhaus type spin texture results in the opposite sign in $\chi_{\rm SO}$ as shown in Eq. (2.45), and also plotted in Fig. 2.7. We see the positive step function for the former and the negative step function in the latter. This is essentially the same behavior as the discrete steps found in 2DEG with Rashba and Dresselhaus SOC in Figs. 2.5 and 2.6.

In the material with large $|g|$ factor, i.e. GaAs, with $m/m0 = 0.067, g = -0.44, g_m =$

-0.015 we will have large value of $\chi_{\rm spin}$ and $\chi_{\rm SO}$.[36] Refer to the results in Fig. 2.5, the magnetic susceptibility will be paramagnetic for negative Fermi energy and diamagnetic for positive Fermi energy.

From the above results, we conclude that the spin texture in the momentum space is crucial for the sign of $\chi_{\rm SO}$, and it deeply influences the observed total susceptibility. In the next section, we calculate the magnetic response in the Dirac / Weyl semimetals and also demonstrate that the spin-momentum relationship is important in those systems.

Chapter 3

3D Dirac/Weyl Semimetal

In this chapter, we calculate magnetic susceptibility in 3D Dirac semimetal and Weyl semimetal. We first introduce 4×4 Hamiltonian which covers the Dirac semimetal, Weyl semimetal as well as the gapped semiconductor. Then we applied the general formulation in the previous section to the Hamiltonian, and analytically obtain the three susceptibility components: spin-spin term, the orbital-orbital term, and the spin-orbital cross term. We also consider the Hamiltonian with the opposite chirality in the spin texture, and argue about how it affects the magnetic susceptibility.

3.1 Electronic Structures of Dirac and Weyl Semimetals

3.1.1 Band dispersion at Zero Magnetic Field

We will introduce 4×4 Dirac-Weyl Hamiltonian matrix. In the absence of the magnetic field the Hamiltonian is,

$$H = \begin{bmatrix} m+b & 0 & vp_z & v(p_x - ip_y) \\ 0 & m-b & v(p_x + ip_y) & -vp_z \\ vp_z & v(p_x - ip_y) & -m+b & 0 \\ v(p_x + ip_y) & -vp_z & 0 & -m-b \end{bmatrix}, \tag{3.1}$$

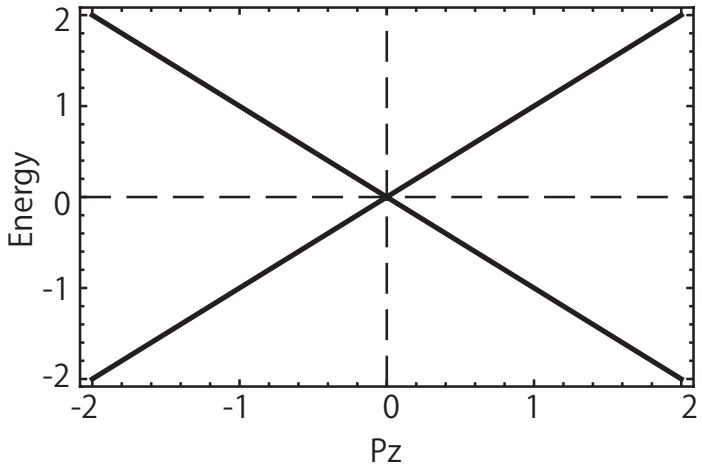

Figure 3.1: Energy spectrum for Dirac semimetal case.m and b are equal to zero. Where v is taken as 1.

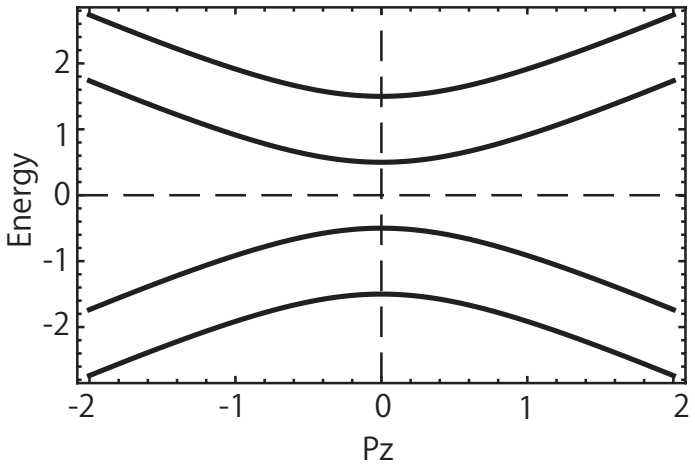

Figure 3.2: Energy spectrum for semiconducting case ($m = 1$, $b = 0.5$). Where v is taken as 1. The spectrum is fully gapped.

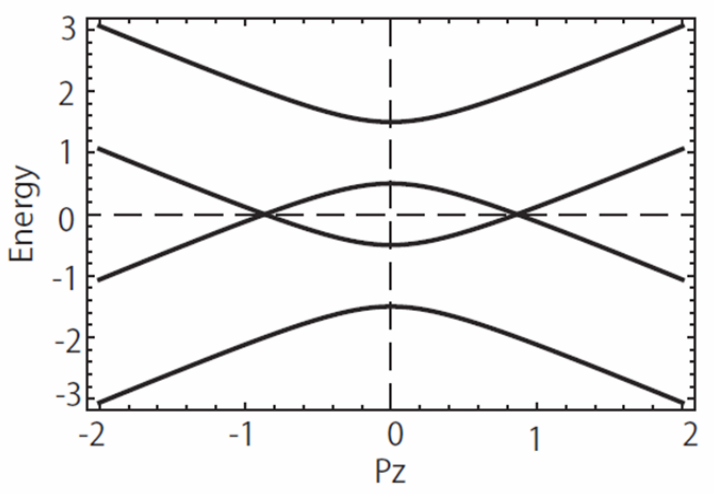

Figure 3.3: Energy spectrum for Weyl semimetal case ($m = 0.5$, $b = 1$). The two bands are touching in $\mathbf{p} = (0, 0, \pm\sqrt{b^2 - m^2}/v)$. Where v is taken as 1.

where m is an effective mass, v is the velocity parameter, and b is the intrinsics Zeeman-like term coupled to the electronic spin, which may exist in magnetic materials without the time-reversal symmetry. We assume $m > 0$ and $b > 0$ in the following. By diagonalizing the Hamiltonian matrix, we obtain the energy spectrum as,

$$\varepsilon(\mathbf{p}) = \pm\sqrt{m^2 + b^2 + v^2p^2 \pm 2b\sqrt{v^2p_z^2 + m^2}}. \tag{3.2}$$

For the case of $p_x = p_y = 0$, we will have the energy spectrum in p_z direction which is given by

$$\varepsilon(0, 0, p_z) = \pm|b| \pm \sqrt{v^2p_z^2 + m^2}. \tag{3.3}$$

The energy spectrum $\varepsilon(0, 0, p_z)$ is plotted in Figs. 3.1, 3.2 and 3.3 for three different cases of $m = b = 0$, $m > b$ and $b > m$, respectively. The case of $m = b = 0$ is the Dirac semimetal, where we have the four-fold degeneracy at the zero energy and the dispersion is completely linear. The second one $m > b$ describes the semiconducting case where the spectrum is gapped in the energy range between $E = m - b$ and $-m + b$. The last one $b > m$ is the Weyl semimetal case where the the middle two bands touching at the wave points $\mathbf{p} = (0, 0, \pm\sqrt{b^2 - m^2}/v)$.

3.1.2 Landau Level Structures

In the case of the presence of magnetic field B perpendicular to z axis, the Hamiltonian 3.1 becomes,

$$H = \begin{bmatrix} m+b & 0 & v\pi_z & v(\pi_x - i\pi_y) \\ 0 & m-b & v(\pi_x + i\pi_y) & -v\pi_z \\ v\pi_z & v(\pi_x - i\pi_y) & -m+b & 0 \\ v(\pi_x + i\pi_y) & -v\pi_z & 0 & -m-b \end{bmatrix}, \tag{3.4}$$

where

$$\boldsymbol{\pi} = \mathbf{p} + e\mathbf{A}, \tag{3.5}$$

and $\mathbf{A}$ is vector potential giving in the magnetic field by $\mathbf{B} = \nabla \times \mathbf{A}$. Here note that b is also dependent on the external magnetic field B as

$$b = b_0 + g\mu_B B, \tag{3.6}$$

where b_0 is the intrinsic Zeeman term in the absence of B, and g is g-factor and $\mu_B = e\hbar/(2m_0)$ is the Bohr magneton, and m_0 is the bare electron mass. We define a lower and uppering operators,

$$a^\dagger = \frac{1}{\sqrt{2e\hbar B}}(\pi_x + i\pi_y) \tag{3.7}$$

$$a = \frac{1}{\sqrt{2e\hbar B}}(\pi_x - i\pi_y), \tag{3.8}$$

which operate on the Landau-level wave function ϕ_n as $a\phi_n = \sqrt{n}\phi_{n-1}$ and $a^\dagger\phi_n = \sqrt{n+1}\phi_{n+1}$. The eigenfunction can be written as $(c_1\phi_{n-1}, c_2\phi_n, c_3\phi_{n-1}, c_4\phi_n)$ for $n \geq 1$, the Hamiltonian matrix for the vector (c_1, c_2, c_3, c_4) then becomes

$$H_{n\leq 1} = \begin{bmatrix} m+b & 0 & vp_z & \Delta_B\sqrt{n} \\ 0 & m-b & \Delta_B\sqrt{n} & -vp_z \\ vp_z & \Delta_B\sqrt{n} & -m+b & 0 \\ \Delta_B\sqrt{n} & -vp_z & 0 & -m-b \end{bmatrix}, \tag{3.9}$$

where

$$\Delta_B = \sqrt{2\hbar v^2 eB}. \tag{3.10}$$

This gives the four energy levels

$$\varepsilon_{s\mu p_z n} = s\sqrt{m^2 + b^2 + v^2 p_z^2 + \Delta_B^2 n + \mu 2b\sqrt{v^2 p_z^2 + m^2}} \tag{3.11}$$

where $s, \mu = \pm$. For $n = 0$, the wave function is written as $(0,\ c_2\phi_0,\ 0,\ c_4\phi_0)$ and the Hamiltonian matrix for (c_2, c_4) becomes

$$H_{n=0} = \begin{bmatrix} m+b & vp_z \\ vp_z & -m+b \end{bmatrix}, \tag{3.12}$$

which gives the only two levels

$$\varepsilon_{\mu p_z 0} = b + \mu\sqrt{v^2 p_z^2 + m^2}, \tag{3.13}$$

with $\mu = \pm$. The level $\varepsilon_{\mu p_z 0}$ can be viewed as the $n = 0$ part of $\varepsilon_{s\mu p_z n}$ in Eq. (3.11), but either of $s = \pm$ branches is missing.

The Landau level spectrum is plotted against p_z in Figs. 3.4, 3.5 and 3.6 for $m = b = 0$, $m > b$ and $b > m$, respectively. We note that the Landau levels of $n \leq 1$ [Eq. (3.11)] is completely electron-hole symmetric with respect to the zero energy because the existence of $s = \pm$ branches, while that of $n = 0$ [Eq. (3.13)] is not symmetric except for $b = 0$. The dashed curves in the figures indicate the energy level $-\varepsilon_{\mu 0}$ which actually does not exist. As we will see in the following sections, the symmetry breaking of $n = 0$ level is actually responsible for the electron-hole asymmetric term in the magnetic susceptibility.

3.2 Formula to Calculate Magnetic Susceptibility

3.2.1 Decomposition of susceptibility

In the following we will calculate analytically the magnetic susceptibility of the Dirac-Weyl Hamiltonian.

The thermodynamic potential is written as

$$\Omega = -\frac{1}{\beta}\frac{1}{2\pi l_B^2}\int_{-\infty}^{\infty}\frac{dp_z}{2\pi\hbar}\sum_{s=\pm}\sum_{\mu=\pm}\sum_{n=0}^{\infty}\varphi[\varepsilon_{s\mu p_z}(x_n)]\left(1 - \delta_{n0}\frac{1-\tau_{s\mu p_z}}{2}\right), \tag{3.14}$$

where

$$\varphi(\varepsilon) = \ln[1 + \exp -\beta(\varepsilon - \zeta)], \tag{3.15}$$

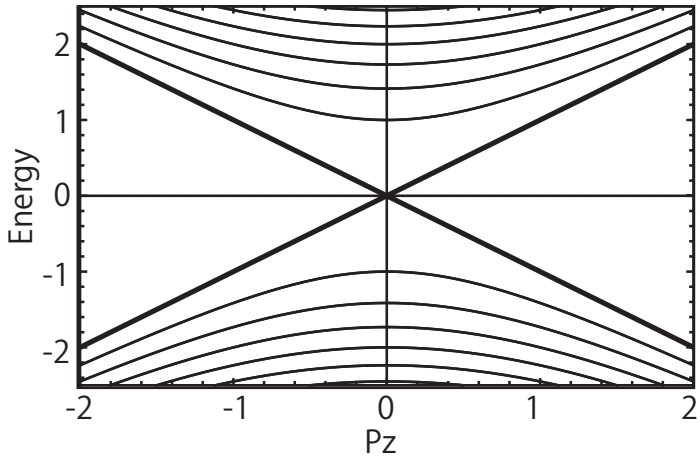

Figure 3.4: Landau level energy spectrum for $m = b = 0$.

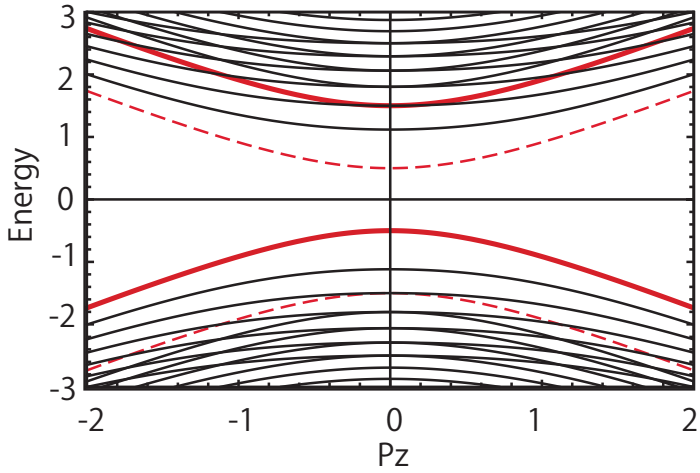

Figure 3.5: Landau level energy spectrum for $m = 1, b = 0.5$. The dashed line is non exist energy level.

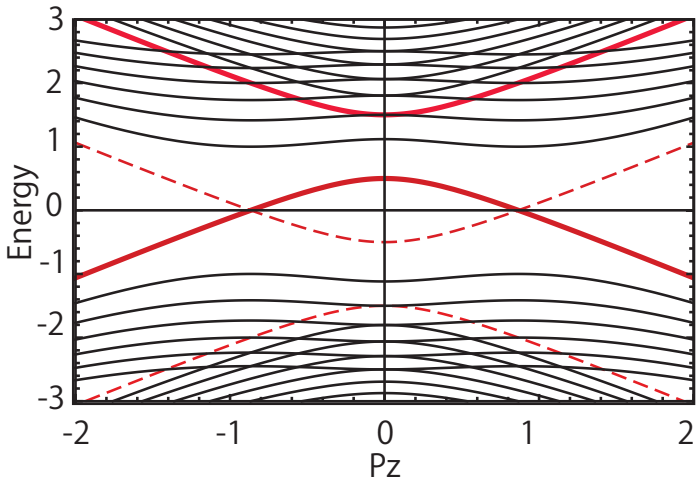

Figure 3.6: Landau level energy spectrum for $m = 0.5, b = 1$. The dashed line is non exist energy level.

$l_B = \sqrt{\hbar/(eB_{\rm orb})}$ is the magnetic length, ζ is the chemical potential, and we defined

$$\begin{aligned} \varepsilon_{s\mu p_z}(x_n) &= \varepsilon_{s\mu p_z n} \\ &= s\sqrt{m^2 + b^2 + v^2 p_z^2 + x_n + \mu 2b\sqrt{v^2 p_z^2 + m^2}} \end{aligned} \tag{3.16}$$

with

$$x_n = n\Delta x, \quad \Delta x \equiv \Delta_B^2 = 2\hbar v^2 e B_{\rm orb}. \tag{3.17}$$

We also introduced the variable $\tau_{s\mu p_z} = \pm 1$ as

$$\tau_{s\mu p_z} = \begin{cases} 1 & \text{when } \varepsilon_{s\mu p_z 0} = \varepsilon_{\mu p_z 0}, \\ -1 & \text{when } \varepsilon_{s\mu p_z 0} = -\varepsilon_{\mu p_z 0}. \end{cases} \tag{3.18}$$

Equivalently, we have $\tau_{s\mu p_z} = +1$ when the Landau level sequence of (s, μ, p_z) start from $n = 0$, while $\tau_{s\mu p_z} = -1$ when it start from $n = 1$ (i.e., the $n = 0$ level is missing).

In weak magnetic field, the summation over n in Eq. (3.14) can be written as a continuous integral over variable x, and additional terms can be Taylor-expanded in $B_{\rm orb}$. For convenience, we introduce the notation,

$$F(x) = \varphi[\varepsilon_{s\mu p_z}(x)]. \tag{3.19}$$

By using the Euler-Maclaurin formula, we can rewrite the summation over n in the case of $\tau_{s\mu p_z} = 1$ (i.e., n starts from 0) as,

$$\sum_{n=0}^{\infty} F(x_n) = \frac{1}{\Delta x}\left[\int_0^{\infty} F(x)dx + F(0)\frac{\Delta x}{2} - F'(0)\frac{\Delta x^2}{12} + \mathcal{O}(\Delta x^3)\right] \quad (3.20)$$

and in the case of $\tau_{s\mu p_z} = -1$ (i.e., n starts from 1) as,

$$\sum_{n=1}^{\infty} F(x_n) = \frac{1}{\Delta x}\left[\int_0^{\infty} F(x)dx - F(0)\frac{\Delta x}{2} - F'(0)\frac{\Delta x^2}{12} + \mathcal{O}(\Delta x^3)\right] \quad (3.21)$$

The two expressions are united into a single equation as

$$\sum_{n=0}^{\infty} F(x_n)\left(1 - \delta_{n0}\frac{1-\tau_{s\mu p_z}}{2}\right) = \frac{1}{\Delta x}\left[\int_0^{\infty} F(x)dx + \tau_{s\mu p_z}F(0)\frac{\Delta x}{2} - F'(0)\frac{\Delta x^2}{12} + \mathcal{O}(\Delta x^3)\right] \quad (3.22)$$

Noting that $\Delta x \propto B_{\rm orb}$, the thermodynamic potential can be expanded within the second order of $B_{\rm orb}$ as

$$\begin{aligned}\Omega &= -\frac{1}{\beta}\frac{1}{2\pi l_B^2}\frac{1}{\Delta x}\int_{-\infty}^{\infty}\frac{dp_z}{2\pi\hbar}\sum_{s=\pm}\sum_{\mu=\pm} \\ &\quad\times\left[\int_0^{\infty}\varphi[\varepsilon_{s\mu p_z}(x)]dx + \tau_{s\mu p_z}\varphi[\varepsilon_{s\mu p_z}(0)]\frac{\Delta x}{2} - \frac{\partial}{\partial x}\,\varphi[\varepsilon_{s\mu p_z}(x)]|_{x=0}\,\frac{\Delta x^2}{12} + \mathcal{O}(\Delta x^3)\right] \\ &= \Omega_0 + \lambda_1 B_{\rm orb} + \lambda_2 B_{\rm orb}^2 + \mathcal{O}(B_{\rm orb}^3), \end{aligned} \quad (3.23)$$

where

$$\Omega_0 = -\frac{1}{\beta}\frac{1}{4\pi\hbar^2 v^2}\int_{-\infty}^{\infty}\frac{dp_z}{2\pi\hbar}\sum_{s=\pm}\sum_{\mu=\pm}\int_0^{\infty}\varphi[\varepsilon_{s\mu p_z}(x)]dx, \quad (3.24)$$

$$\lambda_1 = -\frac{1}{\beta}\frac{1}{4\pi\hbar^2 v^2}\int_{-\infty}^{\infty}\frac{dp_z}{2\pi\hbar}\sum_{s=\pm}\sum_{\mu=\pm}\tau_{s\mu p_z}\varphi[\varepsilon_{s\mu p_z}(0)]\frac{2\hbar e v^2}{2}, \quad (3.25)$$

$$\lambda_2 = -\frac{1}{\beta}\frac{1}{4\pi\hbar^2 v^2}\int_{-\infty}^{\infty}\frac{dp_z}{2\pi\hbar}\sum_{s=\pm}\sum_{\mu=\pm}(-1)\frac{\partial}{\partial x}\,\varphi[\varepsilon_{s\mu p_z}(x)]|_{x=0}\,\frac{4\hbar^2 e^2 v^4}{12}. \quad (3.26)$$

Finally, the three susceptibility components are written in terms of $\Omega_0, \lambda_1, \lambda_2$ as

$$\chi_{\rm spin} = -\left.\frac{\partial^2\Omega_0}{\partial B_{\rm spin}^2}\right|_{B_{\rm spin}=0}, \quad \chi_{\rm SO} = -\left.\frac{\partial\lambda_1}{\partial B_{\rm spin}}\right|_{B_{\rm spin}=0}, \quad \chi_{\rm orb} = -2\lambda_2. \quad (3.27)$$

3.2.2 Calculation of $\chi_{\rm spin}, \chi_{\rm SO}$, and $\chi_{\rm orb}$

3.2.3 $\chi_{\rm spin}$ term

For zero magnetic field $B_{\rm orb} = 0$, we have

$$\Omega(B_{\rm orb}=0) = -\frac{1}{\beta}\int_{-\infty}^{\infty}\frac{dp_z}{2\pi\hbar}\sum_{s=\pm}\sum_{\mu=\pm}\int_0^{\infty}\frac{dp_x dp_y}{4\pi^2\hbar^2}\varphi[\varepsilon_{s\mu p_z}(v^2(p_x^2+p_y^2)))], \tag{3.28}$$

where

$$\varepsilon_{s\mu p_z}(v^2(p_x^2+p_y^2)) = s\sqrt{v^2(p_x^2+p_y^2)+\Delta_B^2},$$

and,

$$\Delta = b + \mu\sqrt{v^2p_z^2+m^2}, \tag{3.29}$$

$s = \mu$ is $\pm$.

Denote more simply expression for p_x and p_y, we have

$$v^2(p_x^2+p_y^2) \equiv v^2p_\perp \equiv x$$

$$2v^2p_\perp = dx$$

$$\int\int\frac{dp_x dp_y}{(2\pi\hbar)^2} = \int_0^{\infty}\frac{2\pi p_\perp dp_\perp}{(2\pi\hbar)^2} = \int_0^{\infty}\frac{2\pi dx}{2v^2(2\pi\hbar)^2} = \frac{1}{4\pi\hbar^2v^2}\int_0^{\infty}dx$$

.

Then we rewrite Ω_0 as,

$$\Omega(B_{\rm orb}=0) = -\frac{1}{\beta}\int_{-\infty}^{\infty}\frac{dp_z}{2\pi\hbar}\sum_{s=\pm}\sum_{\mu=\pm}\int_0^{\infty}\frac{dx}{4\pi\hbar^2v^2}\varphi[\varepsilon_{s\mu p_z}(x)))], \tag{3.30}$$

To calculate $\chi_{\rm spin}$, we need to take the second derivative of Ω_0. Replace vp_z with Π_z, $\chi_{\rm spin}$ can be written as

$$\begin{aligned}\chi_{\rm spin} &= -\frac{\partial^2\Omega_0}{\partial B_{\rm spin}^2}\\ &= -(g\mu_B)^2\frac{\partial^2\Omega_0}{\partial b^2}\\ &= -\frac{(g\mu_B)^2}{4\pi\hbar^2v^2}(-\frac{1}{\beta})\int_{-\infty}^{\infty}\frac{d\Pi_z}{2\pi\hbar v}\sum_{s=\pm}\sum_{\mu=\pm}\int_0^{\infty}dx\frac{\partial^2}{\partial b^2}\varphi[\varepsilon_{s\mu p_z}(x)))]\end{aligned} \tag{3.31}$$

The first derivative is given by,

$$\begin{aligned}\frac{\partial}{\partial b}\varphi(\varepsilon) &= \frac{e^{-\beta(\varepsilon-\zeta)}}{1+e^{-\beta(\varepsilon-\zeta)}}(-\beta)\frac{\partial\varepsilon}{\partial b} \\ &= (-\beta)f(\varepsilon)\frac{\partial\varepsilon}{\partial b} \end{aligned} \tag{3.32}$$

where

$$f(\varepsilon) = \frac{1}{1+e^{\beta(\varepsilon-\zeta)}} \tag{3.33}$$

and $\varepsilon = \varepsilon_{s\mu p_z}(x)$

The second derivative is given by,

$$\frac{\partial^2}{\partial b^2}\varphi(\varepsilon) = (-\beta)\left(f'(\varepsilon)\left(\frac{\partial\varepsilon}{\partial b}\right)^2 + f(\varepsilon)\frac{\partial^2\varepsilon}{\partial b^2}\right) \tag{3.34}$$

Taking the limit of $T \to 0$ of Eq.(3.34), Eq.(3.31) becomes

$$\begin{aligned}\chi_{\text{spin}} &= -\frac{(g\mu_B)^2}{4\pi\hbar^2v^2}(-\frac{1}{\beta})\int_{-\infty}^{\infty}\frac{d\Pi_z}{2\pi\hbar v}\sum_{s=\pm}\sum_{\mu=\pm}\int_0^{\infty}dx\left(f'(\varepsilon)\left(\frac{\partial\varepsilon}{\partial b}\right)^2 + f(\varepsilon)\frac{\partial^2\varepsilon}{\partial b^2}\right) \\ &= -\frac{(g\mu_B)^2}{4\pi\hbar^2v^2}\int_{-\infty}^{\infty}\frac{d\Pi_z}{2\pi\hbar v}\sum_{s=\pm}\sum_{\mu=\pm}\int_0^{\infty}dx\left(-\delta(\varepsilon-\varepsilon_F)\left(\frac{\partial\varepsilon}{\partial b}\right)^2 + \theta(\varepsilon_F-\varepsilon)\frac{\partial^2\varepsilon}{\partial b^2}\right)\end{aligned} \tag{3.35}$$

The first term is Pauli paramagnetism and the second term is Van-Vleck paramagnetism. Therefore, we can divide the calculation to these two parts:

$$\chi_{\text{spin}} = \chi^P_{\text{spin}} + \chi^V_{\text{spin}}, \tag{3.36}$$

where χ^P_{spin} is a Pauli paramagnetism term, which given by

$$\begin{aligned}\chi^P_{\text{spin}} &= -\frac{(g\mu_B)^2}{4\pi\hbar^2v^2}\int_{-\infty}^{\infty}\frac{d\Pi_z}{2\pi\hbar v}\sum_{s=\pm}\sum_{\mu=\pm}\int_0^{\infty}dx\left(-\delta(\varepsilon-\varepsilon_F)\left(\frac{\partial\varepsilon}{\partial b}\right)^2\right) \\ &= -\frac{(g\mu_B)^2}{4\pi\hbar^2v^2}\int_{-\infty}^{\infty}\frac{d\Pi_z}{2\pi\hbar v}\sum_{s=\pm}\sum_{\mu=\pm}\int_0^{\infty}dx\left(-\delta(\varepsilon-\varepsilon_F)\left(\frac{\Delta}{\varepsilon}\right)^2\right),\end{aligned} \tag{3.37}$$

and χ^V_{spin} is a Van-Vleck paramagnetism term given by

$$\begin{aligned}\chi^V_{\text{spin}} &= -\frac{(g\mu_B)^2}{4\pi\hbar^2v^2}\int_{-\infty}^{\infty}\frac{d\Pi_z}{2\pi\hbar v}\sum_{s=\pm}\sum_{\mu=\pm}\int_0^{\infty}dx\left(\theta(\varepsilon_F-\varepsilon)\frac{\partial^2\varepsilon}{\partial b^2}\right) \\ &= -\frac{(g\mu_B)^2}{4\pi\hbar^2v^2}\int_{-\infty}^{\infty}\frac{d\Pi_z}{2\pi\hbar v}\sum_{s=\pm}\sum_{\mu=\pm}\int_0^{\infty}dx\left(\theta(\varepsilon_F-\varepsilon)\frac{x}{\varepsilon^3}\right).\end{aligned} \tag{3.38}$$

For Dirac semimetal ($b = m = 0$) case, $\mu = \pm$ energy levels are degenerated. If we have the Fermi energy less than zero, we will have only $s = 1$ contribution for our calculation. Therefore, the Eq. (3.37) now is given by

$$\begin{aligned}
\chi^P_{\text{spin}} &= -\frac{(g\mu_B)^2}{4\pi\hbar^2 v^2}\int_{-\infty}^{\infty}\frac{d\Pi_z}{2\pi\hbar v}\sum_{\mu=\pm}\int_0^{\infty}dx\left(-\delta(\varepsilon-\varepsilon_F)\left(\frac{\Pi_z}{\varepsilon}\right)^2\right)\\
&= \frac{(g\mu_B)^2}{4\pi\hbar^2 v^2}\int_{-\varepsilon_F}^{|\varepsilon_F|}\frac{d\Pi_z}{2\pi\hbar v}\sum_{\mu=\pm}\int_0^{\infty}d\varepsilon 2\varepsilon\left(\delta(\varepsilon-\varepsilon_F)\left(\frac{\Pi_z}{\varepsilon}\right)^2\right)\\
&= \frac{(g\mu_B)^2}{8\pi^2\hbar^3 v^3}\frac{8|\varepsilon_F|^2}{3}
\end{aligned} \tag{3.39}$$

and the Eq. (3.38) now is given by,

$$\begin{aligned}
\chi^V_{\text{spin}} &= \frac{(g\mu_B)^2}{4\pi\hbar^2 v^2}\int_{-\varepsilon_c}^{\varepsilon_c}\frac{d\Pi_z}{2\pi\hbar v}\sum_{\mu=\pm}\int_0^{\varepsilon_c^2}dx\left(\theta(\varepsilon_F-\varepsilon)\frac{x}{\varepsilon^3}\right)\\
&= 4\frac{(g\mu_B)^2}{4\pi\hbar^2 v^2}\int_0^{\varepsilon_c}\frac{d\Pi_z}{2\pi\hbar v}\int_0^{\varepsilon_c^2}dx\left(\theta(\varepsilon_F-\varepsilon)\frac{x}{\varepsilon^3}\right)\\
&= 4\frac{(g\mu_B)^2}{4\pi\hbar^2 v^2}\int_0^{\varepsilon_c}\frac{d\Pi_z}{2\pi\hbar v}\int_{\Pi_z}^{\varepsilon_c}d\varepsilon 2\varepsilon\left(\theta(\varepsilon_F-\varepsilon)\frac{(\varepsilon^2-\Pi_z^2)}{\varepsilon^3}\right)\\
&= 8\frac{(g\mu_B)^2}{4\pi\hbar^2 v^2}\left(\int_0^{|\varepsilon_F|}\frac{d\Pi_z}{2\pi\hbar v}\int_{|\varepsilon_F|}^{\varepsilon_c}d\varepsilon\left(1-\frac{\Pi_z^2}{\varepsilon^2}\right)+\int_{|\varepsilon_F|}^{\varepsilon_c}\frac{d\Pi_z}{2\pi\hbar v}\int_{\Pi_z}^{\varepsilon_c}d\varepsilon\left(1-\frac{\Pi_z^2}{\varepsilon^2}\right)\right)\\
&= \frac{(g\mu_B)^2}{8\pi^2\hbar^3 v^3}\left(\frac{8|\varepsilon_c|^2}{3}-\frac{8|\varepsilon_F|^2}{3}\right)
\end{aligned} \tag{3.40}$$

where $\varepsilon_c = vp_c$. From the above results we know that the one of the term of χ_0^V cancels the term of χ_0^P. The remaining term is only dependent of ε_c.

For the next case, we put $m \neq 0$ where b is still equal to zero. The Dirac point in the previous case is not exist because of the appearance of the effective mass here. If we assume the Fermi energy negative and lies inside the gap, the susceptibility will be a constant. Now, if the Fermi energy lies below the gap ($\varepsilon_F < -|m|$) the Eq.(3.37) is given by

$$\chi^P_{\text{spin}} = 8\frac{(g\mu_B)^2}{4\pi\hbar^2 v^2}\int_0^{\sqrt{\varepsilon_F^2-m^2}}\frac{d\Pi_z}{2\pi\hbar v}\frac{\sqrt{\Pi_z^2+m^2}}{|\varepsilon_F|} \tag{3.41}$$

and the Van Vleck term now is given by

$$\begin{aligned}\chi^V_{\rm spin} &= 8\frac{(g\mu_B)^2}{4\pi\hbar^2v^2}\left(\int_0^{\sqrt{\varepsilon_F^2-m^2}}\frac{d\Pi_z}{2\pi\hbar v}\int_{|\varepsilon_F|}^{\varepsilon_c}d\varepsilon\left(1-\frac{(\Pi_z^2+m^2)}{\varepsilon^2}\right)\right.\\ &\quad\left.+\int_{\sqrt{\varepsilon_F^2-m^2}}^{\varepsilon_c}\frac{d\Pi_z}{2\pi\hbar v}\int_{\sqrt{(\Pi_z^2+m^2)}}^{\varepsilon_c}d\varepsilon\left(1-\frac{(\Pi_z^2+m^2)}{\varepsilon^2}\right)\right)\\ &= 8\frac{(g\mu_B)^2}{4\pi\hbar^2v^2}\left(\int_0^{\sqrt{\varepsilon_F^2-m^2}}\frac{d\Pi_z}{2\pi\hbar v}\left(\left(\varepsilon_c+\frac{(\Pi_z^2+m^2)}{\varepsilon_c}\right)-\left(\varepsilon_F+\frac{(\Pi_z^2+m^2)}{\varepsilon_F}\right)\right)\right.\\ &\quad\left.+\int_{\sqrt{\varepsilon_F^2-m^2}}^{\varepsilon_c}\frac{d\Pi_z}{2\pi\hbar v}\left(\left(\varepsilon_c+\frac{(\Pi_z^2+m^2)}{\varepsilon_c}\right)-\left(2\sqrt{\Pi_z^2+m^2}\right)\right)\right) \qquad (3.42)\end{aligned}$$

As well as $b=m=0$ case, Pauli term is canceled by one of Van Vleck terms, and the remaining terms are

$$\chi_{\rm spin} = 8\frac{(g\mu_B)^2}{8\pi^2\hbar^3v^3}m^2\ln\frac{\sqrt{\varepsilon_F^2-m^2}+|\varepsilon_F|}{m}+\chi_{spin}(0) \qquad (3.43)$$

where $\chi_{\rm spin}(0)$ is the constant corresponds to the susceptibility for zero Fermi energy. Here is given by

$$\chi_{\rm spin}(0) = 8\frac{(g\mu_B)^2}{8\pi^2\hbar^3v^3}\int_0^{\varepsilon_c}\frac{d\Pi_z}{2\pi\hbar v}\left(\varepsilon_c+\frac{\Pi_z^2+m^2}{\varepsilon_c}-2\sqrt{\Pi_z^2+m^2}\right). \qquad (3.44)$$

3.2.4 $\chi_{\rm SO}$ term

To obtain $\chi_{\rm SO}$, we have to take the first derivative of λ_1 on $B_{\rm spin}$. We will start from the energy spectrum for $x=0$, which is given by

$$\varepsilon_{s\mu p_z}(0) = s\left|b+\mu\sqrt{v^2p_z^2+m^2}\right|. \qquad (3.45)$$

For more simply calculation, we can convert the above equation to

$$\varepsilon'_{s\mu p_z}(0) = \mu' b + s'\sqrt{v^2p_z^2+m^2} \qquad (3.46)$$

where,

$$\chi_{\rm SO} = -\left.\frac{\partial\lambda_1}{\partial B_{\rm spin}}\right|_{B_{\rm spin}=0} \qquad (3.47)$$

For $T\to 0(B\to\infty)$, we have

$$\begin{aligned}\varphi(\varepsilon) &= \ln(1+\exp-\beta(\varepsilon-\varepsilon_F))\\ &\approx -\beta(\varepsilon-\varepsilon_F)\theta(\varepsilon_F-\varepsilon) \qquad (3.48)\end{aligned}$$

or,

$$-\frac{1}{\beta}\varphi(\varepsilon) = (\varepsilon - \varepsilon_F)\theta(\varepsilon_F - \varepsilon) \tag{3.49}$$

For $\varepsilon_F = 0$,

$$\begin{aligned}
\lambda_1 &= \frac{1}{4\pi\hbar^2 v^2}\int_{-\infty}^{\infty}\frac{dp_z}{2\pi\hbar}\sum_{s'\mu'}(\varepsilon_{s'\mu'p_z} - \varepsilon_F)\theta(\varepsilon_F - \varepsilon_{s'\mu'p_z})\frac{2\hbar e v^2}{2} \\
&= \frac{1}{4\pi\hbar^2 v^2}\int_{-\infty}^{\infty}\frac{dp_z}{2\pi\hbar}\sum_{s'=\pm}(b + s'\sqrt{v^2p_z^2 + m^2})\frac{2\hbar e v^2}{2} \\
&= \frac{1}{4\pi\hbar^2 v^2}\int_{-p_c}^{p_c}\frac{dp_z}{2\pi\hbar}2b\frac{2\hbar e v^2}{2} \\
&= \frac{ep_c b}{2\pi\hbar}
\end{aligned} \tag{3.50}$$

For $0 < \varepsilon_F < (b - m)$

Define,

$$\begin{aligned}
|p_+| &= \sqrt{(\varepsilon + b)^2 - m^2}/v \\
|p_-| &= \sqrt{(\varepsilon - b)^2 - m^2}/v
\end{aligned} \tag{3.51}$$

Then,

$$\lambda_1 = \frac{1}{4\pi\hbar^2 v^2}\int_{-p_c}^{p_c}\frac{dp_z}{2\pi\hbar}\Lambda(p_z)\frac{2\hbar e v^2}{2} \tag{3.52}$$

For $p_+ < |p_z|$,

$$\begin{aligned}
\Lambda(p_z) &= \sum_{s',\mu'}\mu'(\mu' b + s'\sqrt{v^2p_z^2 + m^2} - \varepsilon_F) \\
&= (b - \sqrt{v^2p_z^2 + m^2} - \varepsilon_F) - (-b - \sqrt{v^2p_z^2 + m^2} - \varepsilon_F) \\
&= 2b
\end{aligned} \tag{3.53}$$

For $p_- < |p_z| < p_+$

$$\begin{aligned}
\Lambda(p_z) &= (b - \sqrt{v^2p_z^2 + m^2} - \varepsilon_F) - (-b + \sqrt{v^2p_z^2 + m^2} - \varepsilon_F) \\
&\quad -(-b - \sqrt{v^2p_z^2 + m^2} - \varepsilon_F) \\
&= 3b - \sqrt{v^2p_z^2 + m^2} + \varepsilon_F
\end{aligned} \tag{3.54}$$

For $|p_z| < p_-$

$$\begin{aligned}
\Lambda(p_z) &= -(-b + \sqrt{v^2p_z^2 + m^2} - \varepsilon_F) - (-b - \sqrt{v^2p_z^2 + m^2} - \varepsilon_F) \\
&= 2b + 2\varepsilon_F
\end{aligned} \tag{3.55}$$

Then we have,

$$\begin{aligned}
\lambda_1 &= \frac{1}{4\pi\hbar^2 v^2}\int_{-p_c}^{p_c}\frac{dp_z}{2\pi\hbar}\Lambda(p_z)\frac{2\hbar e v^2}{2} \\
&= \frac{1}{4\pi\hbar^2 v^2}(2)\int_{0}^{p_c}\frac{dp_z}{2\pi\hbar}\Lambda(p_z)\frac{2\hbar e v^2}{2} \\
&= \frac{1}{4\pi\hbar^2 v^2}\frac{1}{2\pi\hbar}(2)\left[\int_0^{p_-} dp_z(2b+2\varepsilon_F)+\int_{p_-}^{p_+} dp_z(3b-\sqrt{v^2p_z^2+m^2}+\varepsilon_F)\right. \\
&\quad \left.+\int_{p_+}^{p_c} dp_z 2b\right]\frac{2\hbar e v^2}{2} \\
&= \frac{1}{4\pi\hbar^2 v^2}\frac{1}{2\pi\hbar}(2)\left[(2b+2\varepsilon_F)p_- + (3b+\varepsilon_F)(p_+-p_-)+2b(p_c-p_+)\right. \\
&\quad \left.-\int_{p_-}^{p_+} dp_z\sqrt{v^2p_z^2+m^2}\right]\frac{2\hbar e v^2}{2} \qquad (3.56)
\end{aligned}$$

For $(b-m)<\varepsilon_F<(b+m)$

Define,

$|p_+|=\sqrt{(\varepsilon+b)^2-m^2}/v$

For $p_+<|p_z|$,

$$\begin{aligned}
\Lambda(p_z) &= (b-\sqrt{v^2p_z^2+m^2}-\varepsilon_F)-(-b-\sqrt{v^2p_z^2+m^2}-\varepsilon_F) \\
&= 2b \qquad (3.57)
\end{aligned}$$

For $|p_z|<p_+$

$$\begin{aligned}
\Lambda(p_z) &= (b-\sqrt{v^2p_z^2+m^2}-\varepsilon_F)-(-b+\sqrt{v^2p_z^2+m^2}-\varepsilon_F) \\
&\quad -(-b-\sqrt{v^2p_z^2+m^2}-\varepsilon_F) \\
&= 3b-\sqrt{v^2p_z^2+m^2}+\varepsilon_F \qquad (3.58)
\end{aligned}$$

Then we have,

$$\begin{aligned}
\lambda_1 &= \frac{1}{4\pi\hbar^2 v^2}\frac{1}{2\pi\hbar}(2)\left[\int_0^{p_+} dp_z(3b-\sqrt{v^2p_z^2+m^2}+\varepsilon_F)+\int_{p_+}^{p_c} dp_z 2b\right]\frac{2\hbar e v^2}{2} \\
&= \frac{1}{4\pi\hbar^2 v^2}\frac{1}{2\pi\hbar}(2)\left[(3b+\varepsilon_F)p_+ + 2b(p_c-p_+)-\int_0^{p_+} dp_z\sqrt{v^2p_z^2+m^2}\right]\frac{2\hbar e v^2}{2} \\
&\qquad (3.59)
\end{aligned}$$

For $\varepsilon_F>(b+m)$

Define,

$$\begin{aligned} |p_+| &= \sqrt{(\varepsilon+b)^2-m^2}/v \\ |p_-| &= \sqrt{(\varepsilon-b)^2-m^2}/v \end{aligned} \tag{3.60}$$

For $p_+ < |p_z|$,

$$\begin{aligned} \Lambda(p_z) &= (b-\sqrt{v^2p_z^2+m^2}-\varepsilon_F)-(-b-\sqrt{v^2p_z^2+m^2}-\varepsilon_F) \\ &= 2b \end{aligned} \tag{3.61}$$

For $p_- < |p_z| < p_+$

$$\begin{aligned} \Lambda(p_z) &= (b-\sqrt{v^2p_z^2+m^2}-\varepsilon_F)-(-b+\sqrt{v^2p_z^2+m^2}-\varepsilon_F) \\ &\quad -(-b-\sqrt{v^2p_z^2+m^2}-\varepsilon_F) \\ &= 3b-\sqrt{v^2p_z^2+m^2}+\varepsilon_F \end{aligned} \tag{3.62}$$

For $|p_z| < p_-$

$$\begin{aligned} \Lambda(p_z) &= (b+\sqrt{v^2p_z^2+m^2}-\varepsilon_F)-(-b+\sqrt{v^2p_z^2+m^2}-\varepsilon_F) \\ &\quad +(b-\sqrt{v^2p_z^2+m^2}-\varepsilon_F)-(-b-\sqrt{v^2p_z^2+m^2}-\varepsilon_F) \\ &= 4b \end{aligned} \tag{3.63}$$

Then we have,

$$\begin{aligned} \lambda_1 &= \frac{1}{4\pi\hbar^2v^2}\frac{1}{2\pi\hbar}(2)\left[(4b)p_- + (3b+\varepsilon_F)(p_+-p_-)+2b(p_c-p_+)\right. \\ &\quad \left.-\int_{p_-}^{p_+}dp_z\sqrt{v^2p_z^2+m^2}\right]\frac{2\hbar ev^2}{2} \end{aligned} \tag{3.64}$$

For semiconducting case $\chi_{\rm SO}$ is given by,

$$\chi_{\rm SO} = -\frac{eg\mu_B}{2\pi^2\hbar^2v}\left(\sqrt{(\varepsilon_F+b)^2-m^2}+2\varepsilon_c\right) \tag{3.65}$$

for $|b-m| < \varepsilon_F < |b+m|$ and,

$$\chi_{\rm SO} = -\frac{eg\mu_B}{2\pi^2\hbar^2v}\left(\sqrt{(\varepsilon_F+b)^2-m^2}+\sqrt{(\varepsilon_F-b)^2-m^2}+2\varepsilon_c\right) \tag{3.66}$$

for $(b+m) < \varepsilon_F$.

For Weyl semimetal case $\chi_{\rm SO}$ is given by,

$$\chi_{\rm SO} = -\frac{eg\mu_B}{2\pi^2\hbar^2v}\left(\sqrt{(\varepsilon_F+b)^2-m^2}+\sqrt{(\varepsilon_F-b)^2-m^2}+2vp_c\right) \tag{3.67}$$

for $(b+m) < \varepsilon_F$.

$$\chi_{\rm SO} = -\frac{eg\mu_B}{2\pi^2\hbar^2 v}\left(\sqrt{(\varepsilon_F+b)^2-m^2}+2vp_c\right) \tag{3.68}$$

for $(b-m) < \varepsilon_F < (b+m)$.

$$\chi_{\rm SO} = -\frac{eg\mu_B}{2\pi^2\hbar^2 v}\left(\sqrt{(\varepsilon_F+b)^2-m^2}-\sqrt{(\varepsilon_F-b)^2-m^2}+2vp_c\right) \tag{3.69}$$

for $0 < \varepsilon_F < (b-m)$

3.2.5 $\chi_{\rm orb}$ term

$$\lambda_2 = -\frac{1}{\beta}\frac{1}{4\pi\hbar^2v^2}\int_{-\infty}^{\infty}\frac{dp_z}{2\pi\hbar}\sum_{s\mu}\frac{\partial}{\partial x}\varphi[\varepsilon_{s\mu p_z}(0)]\frac{(2\hbar ev^2)^2}{12} \tag{3.70}$$

For $T \to 0 (B \to \infty)$, we have

$$-\frac{1}{\beta}\frac{\partial}{\partial x}\,\varphi[\varepsilon_{s\mu p_z}(x)]|_{x=0} = \frac{\theta(\varepsilon_F-\varepsilon_{s\mu p_z}(0))}{2\varepsilon_{s\mu p_z}(0)} \tag{3.71}$$

where,

$$\varepsilon_{s\mu p_z}(0) = s|b+\mu\sqrt{v^2p_z^2+m^2}|$$

or,

$$\varepsilon'_{s'\mu' p_z}(0) = \mu' b + s'\sqrt{v^2p_z^2+m^2}$$

and we have,

$$\lambda_2 = -\frac{1}{\beta}\frac{1}{4\pi\hbar^2v^2}\int_{-\infty}^{\infty}\frac{dp_z}{2\pi\hbar}\sum_{s'\mu'}\frac{\theta(\varepsilon_F-\varepsilon'_{s'\mu' p_z}(0))}{2\varepsilon'_{s'\mu' p_z}(0)}\frac{(2\hbar ev^2)^2}{12} \tag{3.72}$$

For $\varepsilon_F = 0$,

$$\int_{-\infty}^{\infty}dp_z\sum_{s'\mu'}\frac{\theta(\varepsilon_F-\varepsilon'_{s'\mu' p_z}(0))}{2\varepsilon'_{s'\mu' p_z}(0)} = 2\int_0^{p_c}dp_z\Lambda(p_z) \tag{3.73}$$

Introducing

$$|p_0| = \frac{1}{v}\sqrt{b^2-m^2} \tag{3.74}$$

For $|p_z| < p_0$,

$$\Lambda(p_z) = \frac{1}{-b+\sqrt{v^2p_z^2+m^2}} + \frac{1}{-b-\sqrt{v^2p_z^2+m^2}} \tag{3.75}$$

For $|p_z| > p_0$,

$$\Lambda(p_z) = \frac{1}{-b - \sqrt{v^2 p_z^2 + m^2}} + \frac{1}{b - \sqrt{v^2 p_z^2 + m^2}} \tag{3.76}$$

Then,Eq. (3.73) becomes,

$$\begin{aligned}\int_{-\infty}^{\infty} dp_z \sum_{s'\mu'} \frac{\theta(\varepsilon_F - \varepsilon'_{s'\mu' p_z}(0))}{2\varepsilon'_{s'\mu' p_z}(0)} &= 2\left[\int_0^{p_0} dp_z \left(\frac{1}{-b + \sqrt{v^2 p_z^2 + m^2}} + \frac{1}{-b - \sqrt{v^2 p_z^2 + m^2}}\right)\right. \\ &\left. + \int_{p_0}^{p_c} dp_z \left(\frac{1}{-b - \sqrt{v^2 p_z^2 + m^2}} + \frac{1}{b - \sqrt{v^2 p_z^2 + m^2}}\right)\right]\end{aligned} \tag{3.77}$$

For $0 < \varepsilon_F < (b - m)$

Define,

$$\begin{aligned}|p_+| &= \sqrt{(\varepsilon + b)^2 - m^2}/v \\ |p_-| &= \sqrt{(\varepsilon - b)^2 - m^2}/v\end{aligned} \tag{3.78}$$

For $p_+ < |p_z|$,

$$\Lambda(p_z) = \frac{1}{b - \sqrt{v^2 p_z^2 + m^2}} + \frac{1}{-b - \sqrt{v^2 p_z^2 + m^2}} \tag{3.79}$$

For $p_- < |p_z| < p_+$

$$\begin{aligned}\Lambda(p_z) &= \frac{1}{-b + \sqrt{v^2 p_z^2 + m^2}} + \frac{1}{b - \sqrt{v^2 p_z^2 + m^2}} + \frac{1}{-b - \sqrt{v^2 p_z^2 + m^2}} \\ &= \frac{1}{-b - \sqrt{v^2 p_z^2 + m^2}}\end{aligned} \tag{3.80}$$

For $|p_z| < p_-$

$$\Lambda(p_z) = \frac{1}{-b + \sqrt{v^2 p_z^2 + m^2}} + \frac{1}{-b - \sqrt{v^2 p_z^2 + m^2}} \tag{3.81}$$

Then we have,

$$\begin{aligned}\int_{-\infty}^{\infty} dp_z \sum_{s'\mu'} \frac{\theta(\varepsilon_F - \varepsilon'_{s'\mu' p_z}(0))}{2\varepsilon'_{s'\mu' p_z}(0)} &= 2\left[\int_0^{p_-} dp_z \left(\frac{1}{-b + \sqrt{v^2 p_z^2 + m^2}} + \frac{1}{-b - \sqrt{v^2 p_z^2 + m^2}}\right)\right. \\ &+ \int_{p_-}^{p_+} dp_z \left(\frac{1}{-b - \sqrt{v^2 p_z^2 + m^2}}\right) \\ &\left. + \int_{p_+}^{p_c} dp_z \left(\frac{1}{-b - \sqrt{v^2 p_z^2 + m^2}} + \frac{1}{b - \sqrt{v^2 p_z^2 + m^2}}\right)\right]\end{aligned} \tag{3.82}$$

For $(b-m) < \varepsilon_F < (b+m)$

Define,

$|p_+| = \sqrt{(\varepsilon+b)^2 - m^2}/v$

Then we have,

$$\begin{aligned}\int_{-\infty}^{\infty} dp_z \sum_{s'\mu'} \frac{\theta(\varepsilon_F - \varepsilon'_{s'\mu'p_z}(0))}{2\varepsilon'_{s'\mu'p_z}(0)} &= 2\left[\int_{p_+}^{p_c} dp_z \left(\frac{1}{b-\sqrt{v^2p_z^2+m^2}}\right)\right. \\ &\left. + \int_0^{p_c} dp_z \left(\frac{1}{-b-\sqrt{v^2p_z^2+m^2}}\right)\right] \quad (3.83)\end{aligned}$$

For $\varepsilon_F > (b+m)$

$$\begin{aligned}\int_{-\infty}^{\infty} dp_z \sum_{s'\mu'} \frac{\theta(\varepsilon_F - \varepsilon'_{s'\mu'p_z}(0))}{2\varepsilon'_{s'\mu'p_z}(0)} &= 2\left[\int_{p_-}^{p_c} dp_z \left(\frac{1}{-b-\sqrt{v^2p_z^2+m^2}}\right)\right. \\ &\left. + \int_{p_+}^{p_c} dp_z \left(\frac{1}{b-\sqrt{v^2p_z^2+m^2}}\right)\right] \quad (3.84)\end{aligned}$$

Finally, we have the final expression of $\chi_{\rm orb}$ in semiconducting case given by

$$\begin{aligned}\chi_{\rm orb} &= \frac{e}{24\pi^2\hbar^2 v}\frac{1}{\sqrt{|m^2-b^2|}}\left(-2b\arctan\left(\frac{b\varepsilon_c}{\sqrt{|m^2-b^2|(\varepsilon_c^2+m^2)}}\right)\right. \\ &+2\sqrt{|m^2-b^2|}\log(v(\varepsilon_c+\sqrt{\varepsilon_c^2+m^2}) \\ &+b\left(\arctan\left(\frac{\sqrt{\varepsilon_F+b^2)-m^2}}{\sqrt{|m^2-b^2|}}+\arctan\left(\frac{b\sqrt{\varepsilon_F+b^2)-m^2}}{\sqrt{|m^2-b^2|}(\varepsilon_F+b)^2}\right)\right)\right. \\ &\left.+\sqrt{|m^2-b^2|}\log(v(\sqrt{\varepsilon_F+b^2)-m^2}+(\varepsilon_F+b)))\right) \quad (3.85)\end{aligned}$$

for $|b-m| < \varepsilon_F < |b+m|$ and,

$$\begin{aligned}\chi_{\rm orb} &= \frac{e}{24\pi^2\hbar^2 v}\frac{1}{\sqrt{|m^2-b^2|}}\left(-2b\arctan\left(\frac{b\varepsilon_c}{\sqrt{|m^2-b^2|(\varepsilon_c^2+m^2)}}\right)\right. \\ &+2\sqrt{|m^2-b^2|}\log(v(\varepsilon_c+\sqrt{\varepsilon_c^2+m^2}) \\ &+b\left(\arctan\left(\frac{\sqrt{\varepsilon_F+b^2)-m^2}}{\sqrt{|m^2-b^2|}}+\arctan\left(\frac{b\sqrt{\varepsilon_F+b^2)-m^2}}{\sqrt{|m^2-b^2|}(\varepsilon_F+b)^2}\right)\right)\right. \\ &+\sqrt{|m^2-b^2|}\log(v(\sqrt{\varepsilon_F+b^2)-m^2}+(\varepsilon_F+b))) \\ &+b\left(-\arctan\left(\frac{\sqrt{\varepsilon_F-b^2)-m^2}}{\sqrt{|m^2-b^2|}}+\arctan\left(\frac{b\sqrt{\varepsilon_F-b^2)-m^2}}{\sqrt{|m^2-b^2|}(\varepsilon_F-b)^2}\right)\right)\right. \\ &\left.-\sqrt{|m^2-b^2|}\log(v(\sqrt{\varepsilon_F-b^2)-m^2}+(\varepsilon_F-b)))\right) \quad (3.86)\end{aligned}$$

for $(b+m) < \varepsilon_F$.

3.3 Magnetic susceptibility of Dirac-Weyl semimetals

3.3.1 Time-reversal symmetric case ($b = 0$)

In this chapter, we argue about the basic properties of the magnetic susceptibility of Dirac-Weyl semimetal in various choices of (m, b). We first consider the the case of $b = 0$, i.e., in the absence of the intrinsic Zeeman term. The susceptibility components at $T = 0$ are expressed as functions of the Fermi energy ε_F as

$$\begin{aligned}
\chi_{\rm spin}(\varepsilon_F) &= +\frac{e^2 v}{4\pi^2\hbar}\left(\frac{g}{m_0 v^2}\right)^2 m^2\theta(|\varepsilon_F|-m)\ln\frac{\sqrt{\varepsilon_F^2-m^2}+|\varepsilon_F|}{m}+\chi_{\rm spin}(0),\\
\chi_{\rm SO}(\varepsilon_F) &= -\frac{e^2 v}{2\pi^2\hbar}\left(\frac{g}{m_0 v^2}\right)\mathrm{sgn}(\varepsilon_F)\theta(|\varepsilon_F|-m)\sqrt{\varepsilon_F^2-m^2}+\chi_{\rm SO}(0),\\
\chi_{\rm orb}(\varepsilon_F) &= -\frac{e^2 v}{12\pi^2\hbar}\times\begin{cases}\ln\dfrac{2\varepsilon_c}{m} & |\varepsilon_F|<m,\\ \ln\dfrac{2\varepsilon_c}{\sqrt{\varepsilon_F^2-m^2}+|\varepsilon_F|} & |\varepsilon_F|>m.\end{cases}
\end{aligned} \tag{3.87}$$

Here $\chi_{\rm spin}(0)$ and $\chi_{\rm SO}(0)$ are constants which solely depend on the energy cut off ε_c. We should note that these terms may not be physically meaningful because in the real material, the susceptibility generally have some offset which is determined by the whole band structure beyond the present description. In the following, therefore, we argue about relative susceptibility with $\chi_{\rm spin}(0)$ and $\chi_{\rm SO}(0)$ substracted.

The three susceptibility components in Eq. (3.87) are separately plotted as solid curves in Fig.3.7, together with the (90°-rotated) band structure in the top panel. The orbital-orbital term $\chi_{\rm orb}$ is negative and logarithmically decays in higher $|\varepsilon_F|$. It actually corresponds to the orbital diamagnetism in 2D graphene, and equivalent to the previous calculation in 3D [50]. The spin-spin term $\chi_{\rm spin}$ corresponds to the summation of the Pauli and the van Vleck paramagnetism, and it is positive and increases as $|\varepsilon_F|$ becomes larger. Interestingly, the spin-orbital term $\chi_{\rm SO}$ is an odd function of ε_F unlike other two components being even functions, and it monotonically decreases in increasing ε_F. It is because $\chi_{\rm SO}$ is solely contributed by the $n = 0$ Landau level, which is responsible for breaking the electron-hole symmetry as we argued in Chapter 2.

It is also important to note that the three susceptibility components have different

magnitudes. The relative magnitudes are roughly estimated as

$$\frac{\chi_{\rm spin}}{\chi_{\rm orb}} \sim \left(\frac{gE}{m_0 v^2}\right)^2, \quad \frac{\chi_{\rm SO}}{\chi_{\rm orb}} \sim \frac{gE}{m_0 v^2}, \tag{3.88}$$

where E is the energy scale corresponding to ε_F and m. Here m_0 is the bare electron mass which originates from μ_B in the Zeeman term. The typical velocity operator is of the order of 10^5 m/s (e.g., 3×10^5 m/s for TaAs[54]), and then $m_0 v^2$ becomes the order of 100 meV. In the case of moderate ε_F and m much smaller than 100 meV, therefore, we expect $\chi_{\rm orb}$ is dominant so that the system becomes diamagnetic in total.

Finally it is worth to argue the Dirac semimetal case $m = b = 0$. Eq. (3.87) except for the constant terms becomes,

$$\begin{aligned}
\chi_{\rm spin}(\varepsilon_F) &= 0, \\
\chi_{\rm SO}(\varepsilon_F) &= -\frac{e^2 v}{2\pi^2\hbar}\left(\frac{g}{m_0 v^2}\right)\varepsilon_F, \\
\chi_{\rm orb}(\varepsilon_F) &= -\frac{e^2 v}{12\pi^2\hbar}\ln\frac{\varepsilon_c}{|\varepsilon_F|}
\end{aligned} \tag{3.89}$$

which are plotted in Fig.3.7 as dashed curves. There $\chi_{\rm spin}$ completely vanishes, $\chi_{\rm SO}$ becomes a simple linear function, and $\chi_{\rm orb}$ gives a negative logarithmic peaks which diverges at zero Fermi energy.

3.3.2 General cases ($b > 0$)

We plot the result of semiconducting case ($m > b$) in Fig.3.8 where the band structure and the plot of $\chi_{\rm spin}$, $\chi_{\rm SO}$, and $\chi_{\rm orb}$ is shown respectively. Unlike $b = 0$ case, we have kink-like structures in all three terms at $\varepsilon_F = \pm(m+b)$ and $\pm(m-b)$ corresponding to the specific band structure such as band edges, while the overall behavior is similar to $(m = 1, b = 0)$ case in the previous section: The relative $\chi_{\rm spin}$ is paramagentic inside the energy bands. The spin-orbital term susceptibility is again an odd function unlike other two, but not a simple linear function anymore and it is constant inside the gap. $\chi_{\rm orb}$ is diamagnetic and logarithmically decays while it is constant inside the gap.

Lastly, we show the plot of Weyl semimetal case in Fig.3.9. We observe in all three terms the kinks corresponding to the band edges as in the previous gapped case, while the property is now significantly different. Importantly, the diamagnetism $\chi_{\rm orb}$ logarithmically diverges at $\varepsilon_F = 0$ similarly to the Dirac semimetal case ($m = b = 0$),

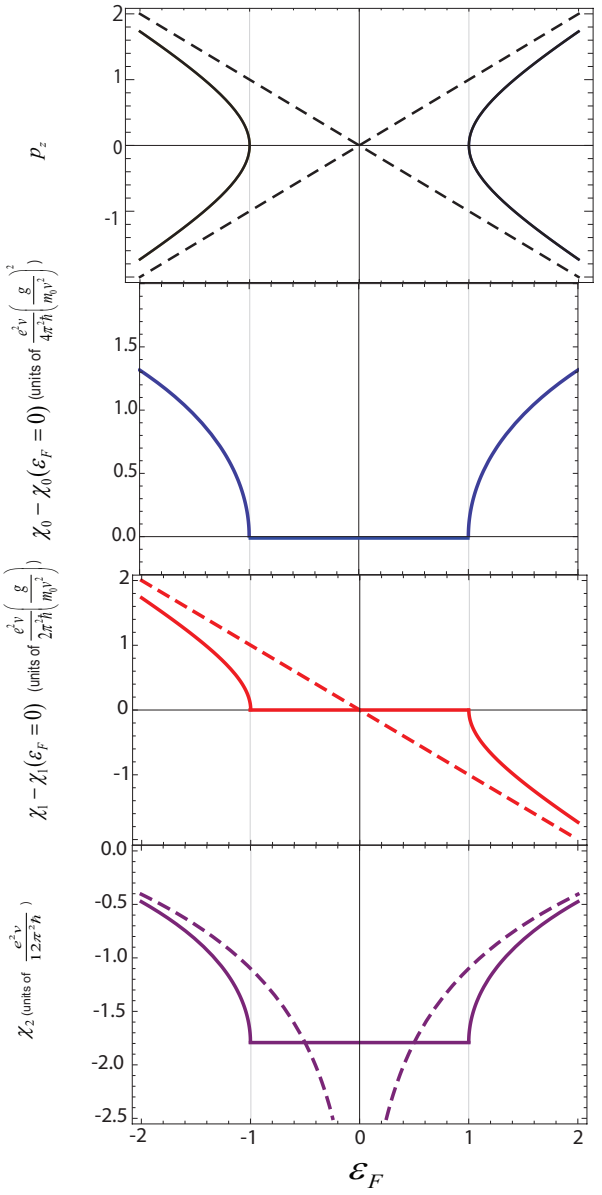

Figure 3.7: Dirac semimetal case ($m = b = 0$; dashed line) and semiconducting case ($m = 1, b = 0$; solid line). (a) Band structure. (b) Spin-spin term susceptibility $\chi_{\text{spin}} - \chi_{\text{spin}}(\varepsilon_F = 0)$. (c) Spin-orbital term susceptibility $\chi_{\text{SO}} - \chi_{\text{SO}}(\varepsilon_F = 0)$. (d) Orbital-orbital term susceptibility χ_{orb}.

and this actually reflects the existence of the linear dispersion around the Weyl nodes at zero energy. In the same region, $\chi_{\rm spin} - \chi_{\rm spin}(\varepsilon_F = 0)$ vanishes and this is also similar to the Dirac semimetal case. Outside the linear band region, $\chi_{\rm spin} - \chi_{\rm spin}(\varepsilon_F = 0)$ becomes negative near the second band edges $\varepsilon_F = \pm(m + b)$, and it increases again outside. $\chi_{\rm SO}$ is rather featureless and monotonically decreases in increasing of Fermi energy.

3.3.3 Chirality Dependence

Similar to the Rashba/Dresselhaus case in the previous section, the sign of the spin-orbit cross susceptibility $\chi_{\rm SO}$ depends on the spin-texture in the momentum space. Here we consider the Hamiltonian,

$$\mathcal{H} = \begin{bmatrix} m+b & 0 & vp_z & v(p_x+ip_y) \\ 0 & m-b & v(p_x-ip_y) & -vp_z \\ vp_z & v(p_x+ip_y) & -m+b & 0 \\ v(p_x-ip_y) & -vp_z & 0 & -m-b \end{bmatrix} \tag{3.90}$$

where $p_x \pm ip_y$ in Eq. (3.1) is inverted to $p_x \mp ip_y$. The difference between Eq. (3.1) and Eq. (3.90) can be understood as the handedness of the spin texture. Specifically, when we go clockwise around the equienergy contour on p_x, p_y plane (i.e., fix p_z), the spin xy component rotates clockwise in Eq. (3.1), while counter-clockwise in Eq. (3.90).

We can calculate the Landau level structures for Eq. (3.90) in the exactly same manner as in Eq. (3.1), then we immediately find that the sign $\tau_{s\mu p_z}$ is inverted: namely, the existing level and non-existing level of n=0 sector are interchanged. All other Landau levels $n \neq 0$ are identical in Eqs. (3.1) and (3.90). As a result, only the spin-orbit cross susceptibility $\chi_{\rm SO}$ inverts its sign from Eq. (3.1), while $\chi_{\rm orb}$ and χ_{spin} remains unchanged. Only the $\chi_{\rm SO}$ is sensitive to the "handedness" of the spin texture, and it affects the total susceptibility.

In Fig.3.10, we plot $\chi_{\rm SO}$ for the Dirac semimetals (with $m = b = 0$) with opposite chiralities, i.e., Eqs. (3.1) and (3.90).

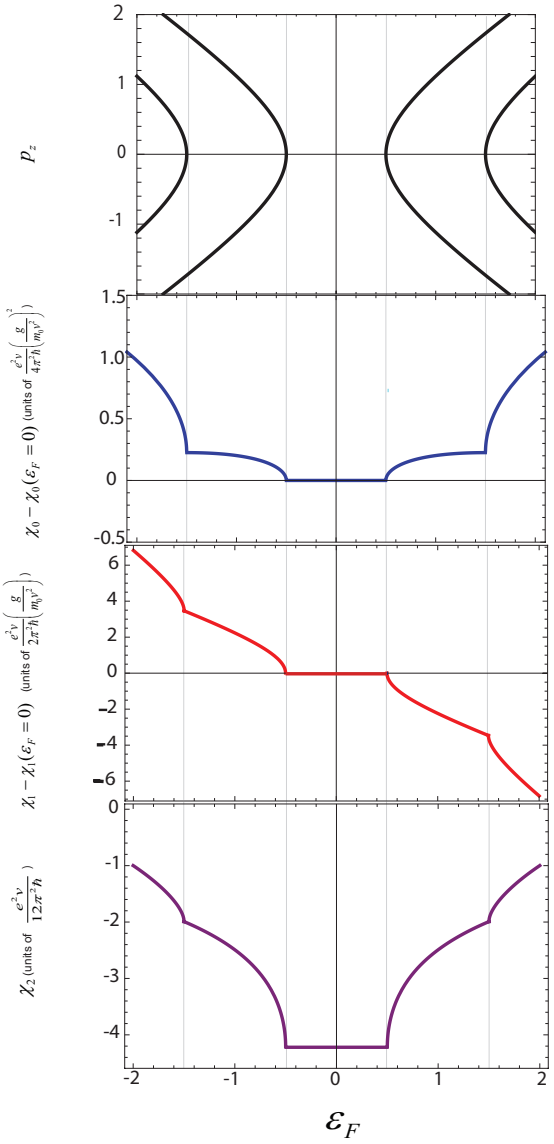

Figure 3.8: General semiconducting case ($m = 1, b = 0.5$). (a) Band structure. (b) Spin-spin term susceptibility $\chi_{\text{spin}} - \chi_{\text{spin}}(\varepsilon_F = 0)$. (c) Spin-orbital term susceptibility $\chi_{\text{SO}} - \chi_{\text{SO}}(\varepsilon_F = 0)$. (d) Orbital-orbital term susceptibility χ_{orb}.

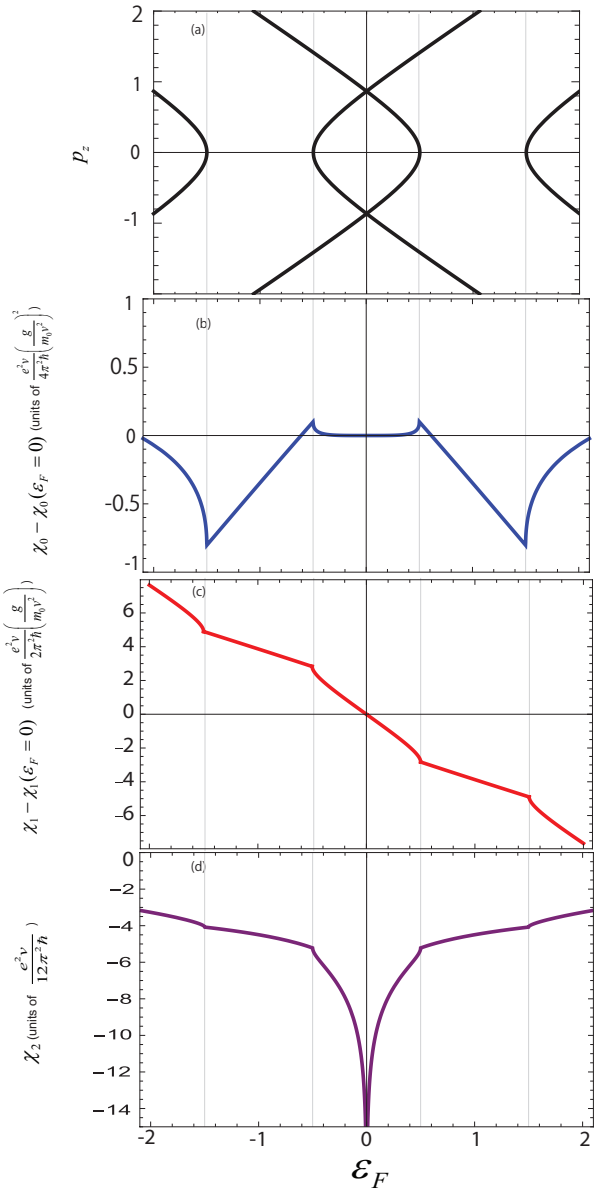

Figure 3.9: Weyl Semimetal Case. $(m = 0.5, b = 1)$. (a) Band structure. (b) Spin-spin term susceptibility $\chi_{\text{spin}} - \chi_{\text{spin}}(\varepsilon_F = 0)$. (c) Spin-orbital term susceptibility $\chi_{\text{SO}} - \chi_{\text{SO}}(\varepsilon_F = 0)$. (d) Orbital-orbital term susceptibility χ_{orb}.

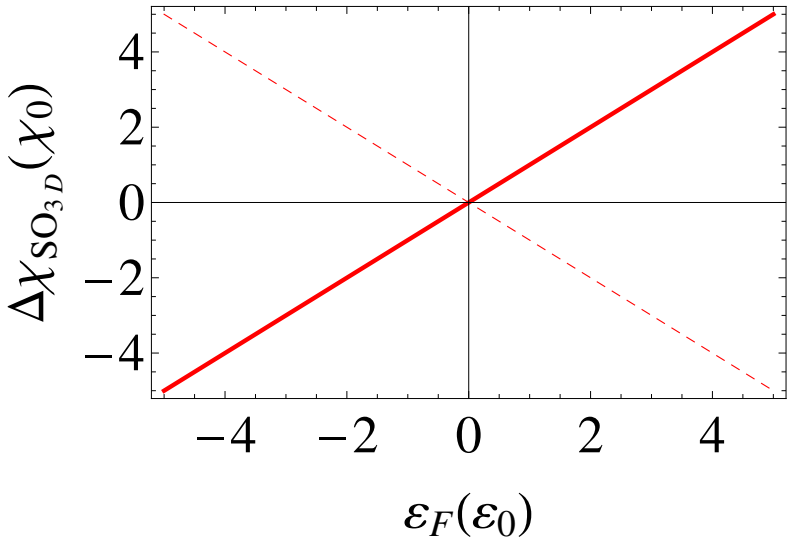

Figure 3.10: χ_{SO} for 3D Dirac semimetal case with opposite chirality. Dashed line for Eq. (3.1) and Solid line for Eq. (3.90).

Chapter 4

Conclusion

In this thesis, We calculated the magnetic susceptibility in various types of materials with spin-orbit coupling, including 2DEG with Rashba / Dresselhaus spin-orbit coupling, 2D Dirac model to describe the surface state of 3D topological insulator, and 3D Dirac / Weyl semimetals. The new findings in the thesis are summarized as follows.

(1) General formulation of the spin-orbit cross susceptibility $\chi_{\rm SO}$.

The conventional knowledge tells us that the magnetic susceptibility is composed of the spin part and orbital part. Here we provided a generic formulation to calculate the magnetic susceptibility from the Landau levels, and found that the materials with spin-orbit coupling generally has the spin-orbit cross susceptibility $\chi_{\rm SO}$ on top of the spin susceptibility $\chi_{\rm spin}$ and orbital susceptibility $\chi_{\rm orb}$. The important point here is that the Hamiltonian depends on the external magnetic field in two different ways, via the orbital term and the spin Zeeman term, and therefore we have three susceptibility components.

(2) Chirality dependence of $\chi_{\rm SO}$.

The Rashba SOC and Dresselhaus SOC have essentially the same energy dispersions, while the spin-texture on the momentum space is different. Specifically, if we rotate the equi-energy contour in the momentum space, then the spin rotates in the opposite directions in Rashba and Dresselhaus systems. One may naively think that the magnetic susceptibility is insensitive to such the chirality (or handedness) of the spin texture, but here we found it is not the case. Namely, the $\chi_{\rm SO}$ is found to have

opposite signs in Rashba and Dresselhaus case, while $\chi_{\rm orb}$ and $\chi_{\rm spin}$ are just identical. We also found that the sign of $\chi_{\rm SO}$ is closely related to the $n = 0$ Landau level, which is also chirality dependent. We applied the same method to the 2D Dirac system and 3D Dirac / Weyl system, and found that the dependence of $\chi_{\rm SO}$ on the chirality of the spin texture is quite general.

(3) Magnetic susceptibility of 3D Dirac / Weyl semimetals.

The Dirac / Weyl semimetals are novel materials attracting much interest in the recent years, while very little was known about the magnetic susceptibility. Here we provided systematic calculations of the magnetic susceptibility for generic 4×4 Hamiltonian, which covers the Dirac semimetal, the Weyl semimetal, and the gapped semiconductor. We calculate the Landau levels and and analytically derive the expression of the magnetic susceptibility. Using the formula, we actually calculated the susceptibility in various different cases.

We found that that $\chi_{\rm orb}$ and $\chi_{\rm spin}$ are even functions of the Fermi energy i.e., electron hole symmetric with respect to zero energy, while only the $\chi_{\rm SO}$ is found to be an odd function of Fermi energy unlike the other two. This makes sense since $\chi_{\rm SO}$ is solely determined by the $n = 0$ Landau level and it breaks the electron hole symmetry. In the Dirac and Weyl semimetal case, in particular, we showed that $\chi_{\rm SO}$ is a monotonically increasing or decreasing function in the Fermi energy, while $\chi_{\rm orb}$ is a logarithmic function which diverges at zero energy. The log divergence is reflects the formation of the band touching points. Using the parameters in experimentally-realized Dirac or Weyl semimetals, we showed that $\chi_{\rm orb}$ is the largest while other terms also have the significant contributions.

We also investigated the susceptibility of the Hamiltonian with opposite chirality in the spin texture, and confirmed that the sign of $\chi_{\rm SO}$ becomes opposite by inverting the chirality, while $\chi_{\rm orb}$ and $\chi_{\rm spin}$ remain unchanged.

Lastly, let us argue about how one can experimentally observe the effects predicted in this thesis. For Rashba / Dresselhaus system, $\chi_{\rm SO}$ governs the total susceptibility in $\varepsilon_F < 0$ (below the Dirac point). If one can measure of the magnetic susceptibility in Rashba/ Dresselhaus system in $\varepsilon_F < 0$, it should be the direct measurement of the chirality dependent part of the magnetic susceptibility. For the surface states of the topological insulator, we predicted the $\chi_{\rm SO}$ jumps at the Dirac point, and its the

direction (negative / positive) depends on the chirality of the spin texture. It should be observed as the jump of the total susceptibility in changing the Fermi energy.

For Weyl / Dirac semimetals, our calculation predicts the strong diamagnetism at the band touching point of Weyl and Dirac semimetal, where the χ_{orb} logarithmically diverges. This should be observed as the dominant part of the magnetism. On the other hand, χ_{SO} is the only term which has different sign in the electron side and the hole side. The present result suggests that the electron side is more paramagnetic or diamagnetic than the hole side, depending on the chirality of the spin texture. So in principle, we can directly detect the chirality by measuring the dependence of the susceptibility on the Fermi energy near the Dirac point. Of course the electron-hole symmetry is generally broken in the real material, and it may also contribute to the electron-hole asymmetry in the susceptibility. The detailed study on this is left for the future work.

Acknowledgments

Fistly, I wish to express my sincere gratitude to my supervisor, Prof. Mikito Koshino, for his patience and for being helpful during my course. Without his helps, I will never finish my research. Secondly, I want to thank Prof. Riichiro Saito for helping me during my doctoral course. I thank all the referees, Prof. Takafumi Sato, Prof. Riichiro Saito, Prof. Takashi Koretsune, and Prof. Naokazu Shibata, for spending their valuable time to refereeing my thesis. I also want to thank all CMPT members for always helping me to be used to study in Tohoku University. Lastly, I would like to thank IGPAS program and MEXT scholarship for giving me a chance to study in Tohoku University.

Bibliography

[1] E. I. Rashba,Sov. Phys. Solid State 2, 1109 (1960).

[2] Yu A. Bychkov and E. Rashba. J. Phys. C: Solid State Phys. 17, 6039 (1984).

[3] G. Dresselhaus. Physical Review 100, 580 (1955).

[4] Liang Fu, C. L. Kane, and E. J. Mele. Topological Insulators in Three Dimensions. PRL 98, 106803 (2007).

[5] J. E. Moore and L. Balents. Topological invariants of time-reversal-invariant band structures. Phys. Rev. B 75, 121306(R),2007.

[6] R. Roy. Topological phases and the quantum spin Hall effect in three dimensions. Phys. Rev. B 79, 195322, 2009.

[7] Hasan, M Zahid and Kane, Charles L. Colloquium: topological insulators. Rev. Mod. Phys.,82(4):3045, 2010.

[8] Xiao-Liang Qi and Shou-Cheng Zhang, Rev. Mod. Phys. 83, 1057 (2011).

[9] Murakami, Shuichi. Phase transition between the quantum spin Hall and insulator phases in 3D: emergence of a topological gapless phase. New J. Phys., 9(9):356, 2007.

[10] Smith, J.C. and Banerjee, S. and Pardo, V. and Pickett, W.E.. Dirac point degenerate with massive bands at a topological quantum critical point. Phys. Rev. Lett., 106(5):056401, 2011.

[11] Yang, Kai-Yu and Lu, Yuan-Ming and Ran, Ying. Quantum Hall effects in a Weyl semimetal: Possible application in pyrochlore iridates. Phys. Rev. B, 84(7):075129, 2011.

[12] Kariyado, Toshikaze and Ogata, Masao. Low-Energy Effective Hamiltonian and the Surface States of Ca_3PbO. J. Phys. Soc. Jpn., 81(6):064701, 2012.

[13] Kariyado, Toshikaze and Ogata, Masao. Three-Dimensional Dirac Electrons at the Fermi Energy in Cubic Inverse Perovskites: Ca_3PbO and Its Family. J. Phys. Soc. Jpn.,80(8):083704, 2011.

[14] Liu, Chao-Xing and Ye, Peng and Qi, Xiao-Liang. Chiral gauge field and axial anomaly in a Weyl semimetal. Phys. Rev. B, 87(23):235306, 2013.

[15] Garate, Ion. Phonon-Induced Topological Transitions and Crossovers in Dirac Materials Phys. Rev. Lett., 110(4):046402, 2013.

[16] Witczak-Krempa, William and Kim, Yong Baek. Topological and magnetic phases of interacting electrons in the pyrochlore iridates. Phys. Rev. B, 85(4):045124, 2012.

[17] Jiang, Jian-Hua. Tunable topological Weyl semimetal from simple-cubic lattices with staggered fluxes Phys. Rev. A, 85(3):033640, 2012.

[18] Xu, Gang and Weng, Hongming and Wang, Zhijun and Dai, Xi and Fang, Zhong. Chern Semimetal and the Quantized Anomalous Hall Effect in $HgCr_2$ Se_4. Phys. Rev. Lett., 107(18):186806, 2011.

[19] Gil Young Cho. Possible topological phases of bulk magnetically doped Bi2Se3: turning a topological band insulator into the Weyl semimetal. arXiv:1110.1939, 2012

[20] M. M. Vazifeh and M. Franz. Electromagnetic Response of Weyl Semimetals. Phys. Rev. Lett., 111:027201, 2013.

[21] Huang, Zhoushen and Das, Tanmoy and Balatsky, Alexander V and Arovas, Daniel P. Stability of Weyl metals under impurity scattering. Phys. Rev. B, 87(15):155123, 2013.

[22] Yang, Kai-Yu and Lu, Yuan-Ming and Ran, Ying. Quantum Hall effects in a Weyl semimetal: Possible application in pyrochlore iridates. Phys. Rev. B, 84(7):075129, 2011.

[23] Halász, Gábor B and Balents, Leon. Time-reversal invariant realization of the Weyl semimetal phase. Phys. Rev. B, 85(3):035103, 2012.

[24] L.D.Landau. Diamagnetism of metals. Z. Phys. 64 629:31-38, (1930).

[25] M. Koshino and I. F. Hizbullah, Physical Review B 93, 045201 (2016).

[26] E G Batyev, Physics, Uspekhi 52 (12) 1245 - 1246 (2009).

[27] Nakai, R. and Nomura, K. Crossed responses of spin and orbital magnetism in topological insulators. Phys. Rev. B, 93:214434, 2016.

[28] J. P. Heida *et al.*, Physical Review B 57, 11911 (1998).

[29] W. T. Wang *et al.*, Applied Physics Letters 91, 082110 (2007).

[30] Christian R. Ast *et al.*, Physical Review Letters 98, 186807 (2007).

[31] K. Ishizaka *et al.*, Nature Materials 10, 521 (2011).

[32] M. Sakano *et al.*, Physical Review Letters 110, 107204 (2013).

[33] J. Yu *et al.*, Nanoscale Research Letters 11, 477 (2016).

[34] S. Souma *et al.*, Scientific Reports 6, 27266 (2016).

[35] G. A. H. Schober *et al.*, Physical Review Letters 108, 247208 (2012).

[36] H. Suzuura and T. Ando, Physical Review B 94, 085303 (2016).

[37] T. Ito and K. Nomura, Unpublished.

[38] M. Koshino and T. Ando, Physical Review B 75, 235333 (2010).

[39] A. Giorgioni *et al.*, Nature Communications 7, 13886 (2016).

[40] Neto, Castro A. H. and Guinea, F. and Peres, N. M. R. and Novoselov, K. S. and Geim, A. K.. The electronic properties of graphene. Rev. Mod. Phys., 81(1): 109–162, 2009.

[41] McClure, J. W.. Diamagnetism of Graphite. Phys. Rev., 104(3):666–671, 1956.

[42] Safran, S. A. and DiSalvo, F. J.. Theory of magnetic susceptibility of graphite intercalation compounds. Phys. Rev. B, 20(12):4889–4895, 1979.

[43] Koshino, Mikito and Ando, Tsuneya. Diamagnetism in disordered graphene. Phys. Rev. B, 75(23):235333, 2007.

[44] Kane, C. L. and Mele, E. J.. Quantum Spin Hall Effect in Graphene. Phys. Rev. Lett., 95(22):226801, 2005

[45] Wan, Xiangang and Turner, Ari M. and Vishwanath, Ashvin and Savrasov, Sergey Y.. Topological semimetal and Fermi-arc surface states in the electronic structure of pyrochlore iridates. Phys. Rev. B, 83(20): 205101, 2011.

[46] Young, S. M. and Zaheer, S. and Teo, J. C. Y. and Kane, C. L. and Mele, E. J. and Rappe, A. M.. Dirac Semimetal in Three Dimensions. Phys. Rev. Lett.,108(14):140405, 2012.

[47] L. Balents. Weyl electrons kiss. Physics, 4:2, 2011.

[48] Ominato, Yuya and Koshino, Mikito. Orbital magnetic susceptibility of finite-sized graphene. Phys. Rev. B, 85(16):165454, 2012.

[49] M. I. D'yakonov and V. Y. Kachorovskii. Spin Relaxation of Two Dimensional Electrons in Noncentrosymetric Semiconductors. Sov. Phys. Semicond. 20, 110 (1986).

[50] Koshino, Mikito and Ando, Tsuneya Anomalous orbital magnetism in Dirac-electron systems: Role of pseudospin paramagnetism. Phys. Rev. B, 81(19):195431, 2010.

[51] Liu, Z. K. and Zhou2, B. and Zhang, Y. and Wang, Z. J. and Weng, H. M. and Prabhakaran, D. and Mo, S.-K. and Shen, Z. X. and Fang, Z. and Dai, X. and Hussain, Z. and Chen, Y. L.. Discovery of a Three-Dimensional Topological Dirac Semimetal, Na3Bi. Science, 343, 2014.

[52] Liu, Z. K. and Jiang, J. and Zhou, B. and Wang, Z. J. and Zhang, Y. and Weng, H. M. and Prabhakaran, D. and Mo, S-K. and Peng, H. and Dudin, P. and Kim,

T. and Hoesch, M. and Fang, Z. and Dai, X. and Shen, Z. X. and Feng, D. L. and Hussain, Z. and Chen, Y. L.. A stable three-dimensional topological Dirac semimetal Cd3As2. Nature Materials, 13:677, 2014.

[53] Lu, Ling and Wang, Zhiyu and Ye, Dexin and Ran, Lixin and Fu, Liang and Joannopoulos, John D. and Soljacic, Marin. Experimental observation of Weyl points. Science, 349(6248): 622-624, 2015.

[54] Lv, B. Q. and Weng, H. M. and Fu, B. B. and Wang, X. P. and Miao, H. and Ma, J. and Richard, P. and Huang, X. C. and Zhao, L. X. and Chen, G. F. and Fang, Z. and Dai, X. and Qian, T. and Ding, H.. Experimental Discovery of Weyl semimetal TaAs. Phys. Rev. X 5, 031013,(2015).

[55] Xu, Su-Yang and Alidoust, Nasser and Belopolski, Ilya and Zhang, Chenglong and Bian, Guang and Chang, Tay-Rong and Zheng, Hao and Strokov, Vladimir and Sanchez, Daniel S and Chang, Guoqing and others. Discovery of a Weyl fermion state with Fermi arcs in niobium arsenide. Nature Physics volume 11, 748-754 (2015).

[56] N. P. Armitage, E. J. Mele, and Ashvin Vishwanath. Weyl and Dirac semimetals in three-dimensional solids Rev. Mod. Phys. 90, 015001, 2018.

[57] Yang, L. X. and Liu, Z. K. and Sun, Y. and Peng, H. and Yang, H. F. and Zhang, T. and Zhou, B. and Zhang, Y. and Guo, Y. F. and Rahn, M. and Dharmalingam, P. and Hussain, Z. and Mo, S. K. and Felser, C. and Yan, B. and Chen, Y. L. Discovery of a Weyl Semimetal in non-Centrosymmetric Compound TaAs. arXiv preprint arXiv:1507.00521, 2015.

[58] Liu, Z. K. and Zhou2, B. and Zhang, Y. and Wang, Z. J. and Weng, H. M. and Prabhakaran, D. and Mo, S.-K. and Shen, Z. X. and Fang, Z. and Dai, X. and Hussain, Z. and Chen, Y. L. Discovery of a Three-Dimensional Topological Dirac Semimetal, Na3Bi. Science, 343, 2014.

[59] Xu, Su-Yang and Xia, Y and Wray, LA and Jia, S and Meier, F and Dil, JH and Osterwalder, J and Slomski, B and Bansil, A and Lin, H and others. Topological phase transition and texture inversion in a tunable topological insulator. Science, 332(6029):560–564,2011.

[60] Mañes, J. L.. Existence of bulk chiral fermions and crystal symmetry. Phys. Rev. B, 85(15):155118, 2012.

[61] Wan, Xiangang and Turner, Ari M and Vishwanath, Ashvin and Savrasov, Sergey Y. Topological semimetal and Fermi-arc surface states in the electronic structure of pyrochlore iridates. Phys. Rev. B, 83(20):205101, 2011.

[62] Young, Steve M and Zaheer, Saad and Teo, Jeffrey CY and Kane, Charles L and Mele, Eugene J and Rappe, Andrew M. Dirac semimetal in three dimensions. Phys. Rev. Lett., 108(14):140405, 2012.

[63] Wang, Zhijun and Sun, Yan and Chen, Xing-Qiu and Franchini, Cesare and Xu, Gang and Weng, Hongming and Dai, Xi and Fang, Zhong. Dirac semimetal and topological phase transitions in A_ {3} Bi (A= Na, K, Rb). Phys. Rev. B, 85(19):195320, 2012.

[64] Singh, Bahadur and Sharma, Ashutosh and Lin, H and Hasan, MZ and Prasad, R and Bansil, A. Topological electronic structure and Weyl semimetal in the TlBiSe_ {2} class of semiconductors. Phys. Rev. B, 86(11):115208, 2012.

[65] Fradkin, Eduardo. Critical behavior of disordered degenerate semiconductors. I. Models, symmetries, and formalism. Phys. Rev. B, 33(5):3257, 1986.

[66] Fradkin, Eduardo. Critical behavior of disordered degenerate semiconductors. II. Spectrum and transport properties in mean-field theory. Phys. Rev. B, 33(5):3263, 1986.

[67] Burkov, AA and Balents, Leon. Weyl semimetal in a topological insulator multilayer. Phys. Rev. Lett., 107(12):127205, 2011.

[68] Burkov, AA and Hook, MD and Balents, Leon. Topological nodal semimetals. Phys. Rev. B, 84(23):235126, 2011.

[69] Kobayashi, Koji and Ohtsuki, Tomi and Imura, Ken-Ichiro and Herbut, Igor F. Density of States Scaling at the Semimetal to Metal Transition in Three Dimensional Topological Insulators. arXiv preprint arXiv:1308.3953, 2013.

[70] Hosur, Pavan and Parameswaran, SA and Vishwanath. Charge transport in Weyl semimetals. Phys. Rev. Lett., 108(4):046602, 2012.

[71] Nandkishore, Rahul and Huse, David A and Sondhi, SL. Dirty Weyl fermions: rare region effects near 3D Dirac points. arXiv:1307.3252, 2013.

[72] Kobayashi, Koji and Ohtsuki, Tomi and Imura, Ken-Ichiro and Herbut, Igor F.. Density of States Scaling at the Semimetal to Metal Transition in Three Dimensional Topological Insulators. Phys. Rev. Lett., 112(1):016402, 2014.

[73] Biswas, Rudro R and Ryu, Shinsei. Diffusive transport in Weyl semimetals. arXiv:1309.3278, 2013.

[74] Noro, Masaki and Koshino, Mikito and Ando, Tsuneya. Theory of Transport in Graphene with Long-Range Scatterers. J. Phys. Soc. Jpn., 79(9):094713, 2010.

[75] Ludwig, Andreas WW and Fisher, Matthew PA and Shankar, R and Grinstein, G. Integer quantum Hall transition: An alternative approach and exact results. Phys. Rev. B, 50(11):7526, 1994.

[76] Shon, Nguyen Hong and Ando, Tsuneya. Quantum transport in two-dimensional graphite system. J. Phys. Soc. Jpn.,67(7):2421–2429, 1998.

[77] Ziegler, K.. Delocalization of 2D dirac fermions: The role of a broken supersymmetry. Physical Rev. Lett.,80(14):3113, 1998.

[78] Katsnelson, MI. Zitterbewegung, chirality, and minimal conductivity in graphene. Eur. Phys. J. B., 51(2):157–160, 2006.

[79] Tworzydło, J and Trauzettel, Björn and Titov, M and Rycerz, Adam and Beenakker, Carlo WJ. Sub-Poissonian shot noise in graphene. Physical Rev. Lett.,96(24):246802, 2006.

[80] Novoselov, KSA and Geim, Ak K and Morozov, SVb and Jiang, Da and Grigorieva, MI Katsnelson IV and Dubonos, SV and Firsov, AA. Two-dimensional gas of massless Dirac fermions in graphene. Nature,438(7065):197–200, 2005.

[81] Zhang, Yuanbo and Tan, Yan-Wen and Stormer, Horst L and Kim, Philip. Experimental observation of the quantum Hall effect and Berry's phase in graphene. Nature,438(7065):201–204,2005.

[82] Ando, T.. Theory of Electronic States and Transport in Carbon Nanotubes. J. Phys. Soc. Jpn., 74(3):777–817, 2005.

[83] Neto, A.H. Castro and Guinea, F. and Peres, N.M.R. and Novoselov, Kostya S. and Geim, Andre K.. The electronic properties of graphene. Rev. Mod. Phys.,81(1):109, 2009.

[84] Shinya Katayama and Akito Kobayashi and Yoshikazu Suzumura. Pressure-Induced Zero-Gap Semiconducting State in Organic Conductor α-(BEDT-TTF)$_2$I$_3$ Salt. J. Phys. Soc. Jpn., 75(5):054705, 2006.

[85] Nielsen, Holger Bech and Ninomiya, Masao. Absence of neutrinos on a lattice:(I). Proof by homotopy theory Nucl. Phys. B, 185(1): 20–40, 1981.

[86] Nielsen, Holger Bech and Ninomiya, Masao. Absence of neutrinos on a lattice:(II). Intuitive topological proof. Nucl. Phys. B, 193(1):173–194, 1981.

[87] McClure, J.W. Diamagnetism of graphite. Phys. Rev., 104(3):666, 1956.